AD-766 559

SEISMIC DISCRIMINATION

David Davies

Massachusetts Institute of Technology

Prepared for:

Advanced Research Projects Agency
Electronic Systems Division

15 August 1973
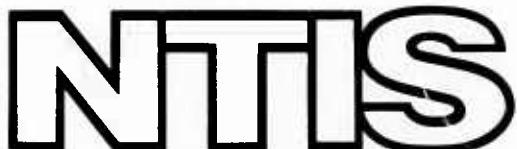
AD 766559

Semiannual Technical Summary

Seismic Discrimination

30 June 1973

Lincoln Laboratory

MASSACHUSETTS INSTITUTE OF TECHNOLOGY

LEXINGTON, MASSACHUSETTS

Approved for public release; distribution unlimited.

DOCUMENT CONTROL DATA – R&D

(Security classification of title, body of abstract and indexing annotation must be entered when the overall report is classified)

1. ORIGINATING ACTIVITY (Corporate author)	2a. REPORT SECURITY CLASSIFICATION
Lincoln Laboratory, M.I.T.	Unclassified
	2b. GROUP

3. REPORT TITLE

Seismic Discrimination

4. DESCRIPTIVE NOTES (Type of report and inclusive dates)

Semiannual Technical Summary Report – 1 January through 30 June 1973

5. AUTHOR(S) (Last name, first name, initial)

Davies, David

6. REPORT DATE	7a. TOTAL NO. OF PAGES	7b. NO. OF REFS
30 June 1973	~~80~~ 75	25

8a. CONTRACT OR GRANT NO. F19628-73-C-0002	9a. ORIGINATOR'S REPORT NUMBER(S)
b. PROJECT NO. ARPA Order 512	Semiannual Technical Summary, 30 June 1973
c.	9b. OTHER REPORT NO(S) (Any other numbers that may be assigned this report)
d.	ESD-TR-73-175

10. AVAILABILITY/LIMITATION NOTICES

Approved for public release; distribution unlimited.

11. SUPPLEMENTARY NOTES	12. SPONSORING MILITARY ACTIVITY
None	Advanced Research Projects Agency, Department of Defense

13. ABSTRACT

Progress on both the short- and long-period constituents of the International Seismic Month is reported. Further work on understanding NORSAR's complexities is described. Evidence is given of the impact of lateral heterogeneity within the earth on seismic observations. We describe our first work on evasion and counter-evasion problems.

14. KEY WORDS

seismic discrimination
seismic array

LASA
NORSAR

MASSACHUSETTS INSTITUTE OF TECHNOLOGY

LINCOLN LABORATORY

SEISMIC DISCRIMINATION

SEMIANNUAL TECHNICAL SUMMARY REPORT
TO THE
ADVANCED RESEARCH PROJECTS AGENCY

1 JANUARY – 30 JUNE 1973

ISSUED 15 AUGUST 1973

D D C

SEP 17 1973

B

LEXINGTON $i\alpha$ MASSACHUSETTS

ABSTRACT

Progress on both the short- and long-period constituents of the International Seismic Month is reported. Further work on understanding NORSAR's complexities is described. Evidence is given of the impact of lateral heterogeneity within the earth on seismic observations. We describe our first work on evasion and counter-evasion problems.

CONTENTS

SUMMARY

This is the nineteenth Semiannual Technical Summary report of M.I.T. Lincoln Laboratory's Seismic Discrimination Group. Our work is directed toward the effective use of all available seismological data in determining the United States' capability to detect and identify underground nuclear weapons tests. For several years a technique has existed which successfully identifies a large majority of seismic events of magnitude greater than a certain value. Our concern at present is to find ways to lower this threshold, to understand occasions when the discriminant fails to work, and to identify features within the earth which can degrade our detection and discrimination capability.

For the past 18 months, we have been concentrating attention on the capability of deployed seismic instruments during a period in February – March 1972 known as the International Seismic Month (ISM). We started with an attempt to produce a comprehensive epicenter list based on short-period detections at LASA, NORSAR, selected World-Wide Net stations, Canadian Network stations, and Swedish and U.K.-sponsored arrays. This work required the development of a major new set of computer programs called DADS (Data Analysis and Display System). With the aid of this interactive facility, the epicenter list is near completion; a portion of the final list is shown. In order to produce a satisfactory location which takes into account not only arrival times of compressional phases but also any $dT/d\Delta$ information that arrays may supply, a completely new algorithm has been developed and has been successfully used in reducing data from the ISM. More recently, we have started to collate long-period information which comes from arrays, conventional single stations, and the Lamont-sponsored long-period experiment. Results from this side of the month's study will follow rapidly on completion of the epicenter list.

The Norwegian array, NORSAR, continues to be the subject of much of our attention. The puzzling complexity of short-period P-wave observations across the array is further examined, and order appears to be emerging from some of the complicated recordings of Eastern Kazakh events. First results of an "array diagram" approach to NORSAR's mislocation anomalies are given and they show features very similar to those observed at LASA. Multipath observations of surface waves are described – the location of NORSAR may make it less vulnerable to multipathing.

We continue to have a strong interest in the effects of heterogeneity in the earth on seismic signals. A model of the crust and upper mantle in the western United States has been used for ray tracing of surface waves in order to give some idea of the effect that heterogeneity within a continental region has on LASA's surface wave reporting ability. Further evidence for lateral heterogeneity deep within the earth is presented. Multipathed body waves are reported from an event distant 95° from LASA, and an amplitude anomaly is described for events in the Pacific recorded at LASA. In both cases, some sort of heterogeneity is necessary in the middle or deep mantle to explain the observed phenomena. An analysis of LASA's array diagram, in terms of potential constituents from different depths, is given.

We are devoting an increased amount of our effort to problems of evasion and counter-evasion. Two specific evasive techniques are considered: multiple shots, and hide-in-earthquake. Seismograms have been synthesized to give an idea of what would be needed to mimic complexity and polarity reversals of the depth phase. A seismogram which distorts the $M_s : m_b$ relationship

GLOSSARY

CGS   United States Coast and Geodetic Survey
DADS   Data Analysis and Display System
ISM   International Seismic Month
LASA   Large Aperture Seismic Array
NORSAR   Norwegian Seismic Array
NOS   National Ocean Survey
SATS   Semiannual Technical Summary
WWSSN   World-Wide Standard Seismographic Network

SEISMIC DISCRIMINATION

I. INTERNATIONAL SEISMIC MONTH

A. EPICENTER LIST PREPARATION

International Seismic Month (ISM) activity has been focused on two areas during the past several months. First, it was decided to review all short-period data and issue a revised and more-documented event list. Secondly, the collection and organization of long-period observations were started in earnest. By 30 June 1973, new event lists and long-period observations will have been sent to all active participants.

Previous issues of our event list were deficient in several respects. Hypocenter information was from several unspecified and heterogeneous sources. No quantitative estimates of epicenter quality were supplied. Similar comments could be made about the body wave magnitudes supplied. The new list is considerably improved in these respects.

To facilitate generation and future manipulation of event lists, several major new programs were written to operate in the Data Analysis and Display System (DADS) environment. Notable among these are /RES and /LOC. These two are programs to calculate residuals and to locate events. The core of these programs is advanced subprograms for residual calculation and location. The locate subprogram uses azimuth and velocity observations as well as arrival times. In addition, it can make use of most of the major seismic phases so that no information is discarded. Finally, it supplies a complete four-dimensional space-time error analysis from which hypocenter and epicenter quality can be obtained. More details concerning the subprograms follow.

/RES and /LOC work directly with large data matrices, with each row representing an arrival. Arrivals from many events are mixed together. The data matrix contains a column, GRPNUM, used to indicate which arrivals all go with a single event by assigning the same value to GRPNUM for all of the arrivals for a single event. /RES will calculate time and velocity residuals and enter them into the data, along with the hypocenter used. As arrivals are added or removed, phase assignments changed, event associations changed, etc., it is the task of the DADS data structure and /RES to be certain that all data remain internally self-consistent. Hypocenters may be input by cards or obtained internally from the DADS data base itself.

/LOC is similar to /RES in many ways, but actually locates the event as well. The hypocenter may be automatically accepted and many events processed in batch, or the user can obtain a display preliminary to accepting the location. The display shows various quality factors including the residuals for the starting and final hypocenter. The user may modify parameters, remove arrivals, restrain depth, etc., and rerun the event. Alternatively, he may decide to reject it totally or accept it.

During the past several months, all ISM events have been processed by /RES. The results were reviewed and corrections made to the data. Each event was then processed by /LOC using the corrected data. The results were again reviewed, and /LOC was rerun on any events having further changes. All events on our new list will have been located by /LOC. Events still causing difficulty or with insufficient data will not be included.

1

TABLE I-1

SAMPLE LISTING OF AN ISM EVENT SUMMARY

EVENT	O. DATE	O. TIME	LAT	LONG	DEPTH	SOURCE	IDNUM	AVEM8	MAXM8	MINM8	MAXAX2	MAXAX3	GSIZE	NAT	NV	NATLOC	NVLOC	NAVEM8	NEXM8	CHI2	DEGF
1	02/20/72	00:18:05	29.37	-113.80	0	S	11017	4.47	4.91	3.58	32	48	37	31	2	25	2	9	5	31.7	25
2	02/20/72	01:08:32	-40.06	45.98	0	S	10068	4.54	4.61	4.47	15	66	31	30	1	28	0	4	0	20.1	25
3	02/20/72	01:09:25	-25.90	179.59	0	S	10069	0.00	0.00	0.00	431	604	5	4	1	3	1	0	0	0.2	1
4	02/20/72	01:09:34	-5.04	145.09	93	S	10070	4.28	4.28	4.28	15	29	10	10	0	10	1	1	0	3.1	6
5	02/20/72	02:17:26	-28.98	-66.99	122	S	10137	0.00	0.00	0.00	22	27	9	8	1	8	1	0	0	4.6	6
6	02/20/72	02:20:56	-21.03	-68.61	118	S	10140	3.95	3.97	3.93	150	1.0	8	6	2	6	2	4	0	1.4	6
7	02/20/72	02:32:01	29.58	-113.69	0	SR	10152	4.32	4.99	3.47	31	27	31	28	3	27	3	9	6	23.6	30
8	02/20/72	02:58:13	-17.47	-71.17	120	S	10177	3.49	3.49	3.49	64	41	8	7	1	7	1	2	0	2.9	5
9	02/20/72	03:02:08	34.49	80.30	0	SR	10182	4.88	5.69	3.93	12	51	45	42	3	26	3	19	2	20.3	29
10	02/20/72	03:29:44	-39.98	-75.01	0	SR	10209	4.30	4.48	4.22	54	124	10	9	1	9	1	3	0	17.5	8
11	02/20/72	03:46:48	25.04	122.15	41	S	10228	4.36	4.40	4.35	64	64	9	8	1	8	1	3	2	15.3	6
12	02/20/72	04:00:30	-20.87	-70.48	71	S	10240	4.73	5.41	4.50	12	15	29	27	2	27	2	15	0	15.8	27
13	02/20/72	04:30:42	20.83	120.19	0	SR	10270	4.61	5.00	4.20	8	29	31	30	1	27	1	11	0	13.4	26
14	02/20/72	04:38:14	-26.47	-178.12	228	S	10278	5.09	5.48	4.58	34	96	62	60	2	24	2	8	0	11.1	24
15	02/20/72	04:57:30	29.36	-113.08	197	S	10298	4.42	5.13	3.63	59	86	16	15	1	13	1	5	3	8.3	12
16	02/20/72	05:10:10	35.18	70.52	83	S	10309	3.68	4.43	3.54	46	47	11	5	3	6	2	2	1	3.0	6
17	02/20/72	05:35:51	29.30	-112.68	17	S	10336	3.16	4.28	3.10	249	265	5	5	0	5	0	26	7	0.3	1
18	02/20/72	06:08:15	29.69	-113.45	60	S	10368	5.22	5.91	4.28	18	40	79	76	3	26	3	3	0	9.8	28
19	02/20/72	06:24:02	-39.99	45.90	103	S	10383	4.78	4.93	4.62	10	79	40	40	0	27	0	3	0	8.9	22
20	02/20/72	06:43:44	29.70	-113.28	116	S	10403	4.42	4.89	3.96	94	108	8	8	0	8	0	6	0	3.6	4
21	02/20/72	07:36:58	10.92	-62.09	103	S	10457	4.29	4.75	3.81	16	43	15	14	1	14	1	4	1	5.4	11
22	02/20/72	07:43:25	29.47	-113.61	0	S	10465	3.58	4.76	3.40	75	122	11	10	1	10	1	7	0	1.3	8
23	02/20/72	08:08:15	-28.49	-179.38	0	S	10488	4.58	4.58	4.58	149	307	5	4	1	4	1	1	0	6.2	2
24	02/20/72	08:51:34	29.53	-113.72	0	S	10531	4.27	4.79	3.95	69	101	11	10	1	10	1	3	0	7.3	8
25	02/20/72	09:25:12	30.44	-112.91	71	S	10555	3.78	4.16	3.59	230	256	6	5	1	5	1	4	0	0.3	2
26	02/20/72	10:04:15	18.18	-95.16	135	S	10604	4.60	5.12	4.10	47	47	17	15	2	15	2	14	1	4.0	15
27	02/20/72	10:08:26	42.10	145.88	496	S	10607	4.08	4.82	3.58	22	22	27	24	3	19	3	17	0	6.5	21
28	02/20/72	10:22:32	36.64	78.82	112	S	10622	3.91	4.35	3.60	38	74	11	9	2	8	2	7	1	14.0	8
29	02/20/72	10:52:15	29.48	-113.98	0	SR	10652	3.58	4.52	3.58	283	406	6	5	1	5	0	4	0	1.3	3
30	02/20/72	11:04:06	31.56	-113.14	128	S	10663	3.77	4.33	3.57	96	100	6	5	1	5	1	4	0	2.7	3
31	02/20/72	11:05:30	-3.33	146.35	52	S	10665	0.00	0.00	0.00	34	35	8	8	0	8	0	0	0	1.4	4
32	02/20/72	13:01:56	29.57	-113.62	0	SR	10782	4.34	5.41	3.00	22	36	31	28	3	25	2	13	6	13.8	26
33	02/20/72	13:28:36	-14.35	167.19	136	S	10808	4.79	5.77	4.28	18	18	61	58	3	26	1	11	1	3.8	24
34	02/20/72	13:30:19	28.69	-113.81	0	SR	10810	3.53	3.98	3.53	282	364	9	8	1	6	0	5	0	1.6	8
35	02/20/72	14:10:11	-21.52	169.41	130	S	10849	4.50	5.38	3.33	7	11	49	48	1	28	1	5	0	43.6	26
36	02/20/72	14:26:57	29.65	-113.49	9	S	10866	4.24	4.52	3.99	42	63	14	14	0	14	0	7	1	5.4	10
37	02/20/72	15:20:00	42.62	142.10	55	S	10919	4.03	4.74	3.55	36	68	13	10	3	10	3	7	0	5.1	12
38	02/20/72	15:57:13	30.11	-112.77	26	S	10957	3.05	3.52	2.82	179	266	8	7	1	7	1	4	0	1.1	5
39	02/20/72	16:25:38	-15.35	179.44	510	S	10984	3.96	4.34	3.57	55	243	13	11	2	8	2	7	0	9.3	8
40	02/20/72	16:27:23	29.97	-113.21	40	S	10987	3.84	4.67	3.63	63	72	11	10	1	9	1	3	0	4.2	7
41	02/20/72	17:40:52	-23.91	179.60	700	SR	11059	4.21	4.57	4.03	47	104	9	7	2	7	2	3	1	2.7	8
42	02/20/72	18:06:44	30.41	-113.09	74	S	11086	3.50	4.41	3.48	141	157	7	7	0	7	0	2	0	4.2	5
43	02/20/72	18:09:46	27.60	-115.32	0	S	11090	3.34	4.35	3.34	579	830	8	7	1	7	1	3	0	20.3	3
44	02/20/72	19:28:37	30.58	-112.38	148	S	11168	3.71	4.19	3.40	91	93	8	6	2	8	0	3	0	9.5	4
45	02/2 /72	19:35:54	29.74	-113.39	0	S	11176	3.88	3.88	3.08	994	1391	8	8	0	8	1	3	0	2.6	2
46	02/20/72	19:59:04	29.30	-113.70	0	S	11199	3.25	3.37	3.19	259	378	7	7	0	7	0	1	0	13.2	1
47	02/20/72	20:07:02	51.96	155.73	35	S	11207	4.12	4.50	3.59	33	157	10	10	0	8	2	7	0	0.8	5
48	02/20/72	20:31:36	-6.07	130.32	55	S	11231	4.66	4.66	4.66	21	43	22	18	4	9	2	1	0	2.1	6
49	02/20/72	21:38:40	36.81	21.73	85	S	11298	4.22	5.01	3.92	12	21	15	15	0	15	0	9	2	9.5	17
50	02/20/72	21:54:14	29.67	-113.33	36	S	11314	4.08	4.90	3.38	42	46	12	10	2	14	3	3	2	6.3	10
51	02/20/72	22:05:43	40.04	139.53	53	S	11325	3.93	4.36	3.60	39	82	10	10	0	10	0	3	2	2.5	10
52	02/20/72	22:42:45	22.63	-113.45		SR	11363	3.35	3.93	3.07	1047	1467	3	2	1	2	1	7	0	0.0	1

EVENT = Sequential count

O. DATE = Date

O. TIME = Origin Time

LAT = Latitude

LONG = Longitude

DEPTH = Depth in kilometers

SOURCE = Indicates source of hypocenter: S means it was run free, and SR means depth restrained

IDNUM = Last five digits of the event identification number

AVEM8 = m_b assigned to the event

MAXM8 = Largest reported m_b

MINM8 = Smallest reported m_b

MAXAX2 = Length (in km) of largest epicenter error ellipse semiaxis

MAXAX3 = Length (in km) of largest hypocenter error ellipsoid semiaxis

GSIZE = Number items associated with the event (GSIZE = NAT+NV)

NAT = Number of items which are arrival times

NV = Number of items which are velocities

NATLOC = Number of arrival times used in getting location

NVLOC = Number of velocities used in getting location

NAVEM8 = Number of m_b values averaged to get AVEM8

NEXM8 = Number of m_b values not used in calculating AVEM8 because values were more than 0.6 unit away from AVEM8

CHI2 = Chi-square goodness of fit parameter

DEGF = Degrees of freedom for CHI2

The new event list will include, in addition to hypocenter and origin time:

(1) The largest semiaxes of the epicenter error ellipse and of the hypocenter error ellipsoid.

(2) The number of arrival times and velocities used in location, and the number associated with the event but not used.

(3) An m_b value calculated from amplitude and period data contained in DADS, excluding reports more than 0.5 unit away from the given value.

(4) The number of values averaged to calculate m_b and the number excluded by virtue of being too far from the average.

(5) Minimum and maximum station m_b values.

Detailed corroborating information on any event will be available to participants on request. Table I-1 is a short sample of the kind of event list which will be distributed.

Up to the present, ISM activity with short-period data has been limited to data organization and event list preparation, as outlined above and in previous SATS. However, Fig. I-1 shows our epicenter quality as a function of our m_b values for events during a three-day period. The quality factor (MAXAX2) shown is the maximum principal semiaxis (km) of the epicenter error ellipse. The exact interpretation will require further research, but it is probably very conservative to assert that the true epicenter will be no more than MAXAX2 away from the calculated epicenter with high probability. Note that quality is excellent down to about m_b = 4.5, and then deteriorates quite rapidly. It should be noted that the event at m_b = 4.8 with poor quality actually has m_b determined from only one measurement and that there is poor distance and azimuth control. An important point to note is that one can be automatically informed about potential errors in calculated epicenters. Clearly, interpretation of the ISM data for detection and location will be a considerable challenge.

Long-period readings and measurements have been accumulated from several sources and organized into an integrated data set. Final event associations and analysis have not been undertaken, although preliminary associations by outside participants and Lincoln are indicated in the data base. Several thousand long-period vertical measurements of signal and noise were contributed by Lincoln from visual analysis of some 15 WWSSN stations for the entire time period. The Seismic Array Analysis Center did frequency-wavenumber analysis of selected time periods for the vertical component of the large arrays, and supplied the computer output to Lincoln. These data have been sifted by us and entered into the data base for further interpretation. Insofar as possible, basic observational data from all other participants have been included as furnished by them, but derived quantities (such as M_s values) have not.

R. T. Lacoss
R. M. Sheppard
R. E. Needham

B. DATA ANALYSIS AND DISPLAY SYSTEM (DADS)

The DADS continues to be refined and expanded. Some significant features that have been added are the /SEARC and /PLOT programs which are described below, and programs to compute source locations and residuals for the ISM which are described in Sec. A above.

DADS is an interactive display system designed to operate on tabular data. Generally, the columns are referred to as parameters and have names assigned to them. The rows are events

or arrivals and are numbered sequentially. A selector is a named column that has the special function of flagging certain of the events that form a meaningful subset of the data.

Previously, selectors could only be created by specifying the events by number or by writing a special-purpose Fortran program to choose them. Now, the user merely types in a list of conditions and /SEARC sets up a selector containing all the events which meet those conditions. For example, the user might want to set up a selector BIGEV which consists of events where the magnitude parameter (MB) has a value greater than 5.0 and the station reporting the arrival (A.STA) is either LASA or NORSAR. The command would be:

```
/SEARC
1.  A.STA EQ LAO NAO
2.  MB GT 5.0
SEL=BIGEV 1 2
```

The program stores the conditions typed in and displays them on the scope. The user can thus set up several selectors with different combinations of the same basic conditions without having to retype the conditions each time. A search imposing several conditions on up to 8000 events executes in less than 1 sec.

The /PLOT program produces a scatter plot of any two parameters for the events in a given selector. Scaling may be automatic or preset by the user. The user may optionally control the character plotted for each event by previously setting up a parameter column which contains that character for each event. Figure 1-1 is an example of the output of this program.

L. J. Turek

C. EXTENSION OF STANDARD EVENT LOCATION PROCEDURES

Conventional methods for calculating seismic hypocenter locations make use of only the observed arrival times of the P and PKP phases. This is not too serious a restriction for large events which are widely recorded, but for small events it frequently happens that potentially valuable data are discarded. Array measurements of $dt/d\Delta$ and azimuth, for example, cannot be included. Nor can arrival times of other phases (e.g., S, PKKP, etc.) which often contain significant information, especially on focal depth and origin time. The standard iterative least-squares location method, however, is easily adaptable to include such data.

For use in processing data for the ISM, we have developed a generalized location program which accepts any combination of $dt/d\Delta$-azimuth and/or arrival time data for any phases (for which travel time tables are available). At present, the phases in use are, P, PP, PcP, PKP (A-B, B-C, and D-F branches), PKKP (A-B, B-C, and D-F), P'P' (A-B, B-C, and D-F), S, SS, ScS, SKS (A-C, C-D, and D-F), including depth phases in all cases.

Another deficiency of standard location methods lies in the technique used to estimate the accuracy of calculated hypocenters.[1] The magnitude of the errors of observation is estimated from the quality of the fit to the data, the errors being assumed to be random and uncorrelated. In fact, however, these "errors" are produced primarily by lateral velocity variations in the earth and are thus systematically related to each other and can introduce systematic errors into the calculated locations. In other words, velocity variations in the earth produce travel time anomalies which often can be "canceled out" by a suitable mislocation of the hypocenter, and the resulting internal consistency of the fit to the data may be deceptively good. For explosions with known hypocentral parameters, for example, it usually happens that the true location lies far outside the estimated uncertainty bounds, indicating that such bounds may be severely

4

misleading. Therefore, we have chosen to estimate the probable errors in the data a priori, on the basis of experience with events of known location, etc. These estimates will, of course, be considerably larger than the actual measurement errors, or than the standard deviations of the data relative to a best-fit hypocenter, but they will more realistically represent the true uncertainty in the location.

The basic method for calculating locations is a simple extension of the method first described by Bolt.[2] The (nonlinear) relation between the hypocentral parameters and each observed seismic datum (arrival time or slowness) is expressed in linearized form in terms of changes from some initial values. For an arrival time datum, we get

$$\delta t = \delta t_o + \frac{\partial t}{\partial \Theta_o} \delta \Theta_o + \frac{\partial t}{\partial \varphi_o} \delta \varphi_o + \frac{\partial t}{\partial h_o} \delta h_o \tag{1-1}$$

where

t = arrival time

t_o = origin time

Θ_o = epicentral colatitude

φ_o = epicentral longitude

h_o = focal depth.

The partial derivatives in Eq. (1-1) are given by

$$\frac{\partial t}{\partial \Theta_o} = \frac{\partial T}{\partial \Delta} \frac{\partial \Delta}{\partial \Theta_o} = \frac{\partial T}{\partial \Delta} \cos \zeta_o$$

$$\frac{\partial t}{\partial \varphi_o} = \frac{\partial T}{\partial \Delta} \frac{\partial \Delta}{\partial \varphi_o} = -\frac{\partial T}{\partial \Delta} \sin \Theta_o \cos \zeta_o$$

$$\frac{\partial t}{\partial h_o} = \frac{\partial T}{\partial h_o}$$

where

$T(\Delta, h_o)$ = travel time

Δ = epicentral distance

ζ_o = azimuth from epicenter to station.

A $dt/d\Delta$-azimuth measurement is considered as a vector slowness:

$$p_x = \frac{\partial t}{\partial \Delta} \sin \zeta \qquad p_y = \frac{\partial t}{\partial \Delta} \cos \zeta$$

where ζ is the azimuth from the station to the epicenter. Corresponding to Eq. (1-1), we get

$$\delta p_x = \frac{\partial p_x}{\partial \Theta_o} \delta \Theta_o + \frac{\partial p_x}{\partial \varphi_o} \delta \varphi_o + \frac{\partial p_x}{\partial h_o} \delta h_o$$

$$\delta p_y = \frac{\partial p_y}{\partial \Theta_o} \delta \Theta_o + \frac{\partial p_y}{\partial \varphi_o} \delta \varphi_o + \frac{\partial p_y}{\partial h_o} \delta h_o \quad . \tag{1-2}$$

The necessary partial derivatives are

$$\frac{\partial p_x}{\partial \theta_o} = \frac{\partial T}{\partial \Delta} \cos \zeta \frac{\partial \zeta}{\partial \theta_o} + \frac{\partial^2 T}{\partial \Delta^2} \frac{\partial \Delta}{\partial \theta_o} \sin \zeta$$

$$= -\frac{\partial T}{\partial \Delta} \frac{\cos \zeta \sin \zeta_o}{\sin \Delta} + \frac{\partial^2 T}{\partial \Delta^2} \cos \zeta_o \sin \zeta$$

$$\frac{\partial p_x}{\partial \varphi_o} = \frac{\partial T}{\partial \Delta} \cos \zeta \frac{\partial \zeta}{\partial \varphi_o} + \frac{\partial^2 T}{\partial \Delta^2} \frac{\partial \Delta}{\partial \varphi_o} \sin \zeta$$

$$= -\left[\frac{\partial T}{\partial \Delta} \frac{\cos \zeta_o \cos \zeta}{\sin \Delta} + \frac{\partial^2 T}{\partial \Delta^2} \sin \zeta_o \sin \zeta \right] \sin \theta_o$$

$$\frac{\partial p_x}{\partial h_o} = \frac{\partial^2 T}{\partial h_o \partial \Delta} \sin \zeta$$

and similarly

$$\frac{\partial p_y}{\partial \theta_o} = \frac{\partial T}{\partial \Delta} \frac{\sin \zeta_o \sin \zeta}{\sin \Delta} + \frac{\partial^2 T}{\partial \Delta^2} \cos \zeta_o \cos \zeta$$

$$\frac{\partial p_y}{\partial \varphi_o} = \left[\frac{\partial T}{\partial \Delta} \frac{\cos \zeta_o \sin \zeta}{\sin \Delta} - \frac{\partial^2 T}{\partial \Delta^2} \sin \zeta_o \cos \zeta \right] \sin \theta_o$$

$$\frac{\partial p_y}{\partial h_o} = \frac{\partial^2 T}{\partial h_o \partial \Delta} \cos \zeta$$

In the foregoing, we have made use of the relations

$$\frac{\partial \Delta}{\partial \theta_o} = \cos \zeta_o$$

$$\frac{\partial \Delta}{\partial \varphi_o} = - \sin \theta_o \sin \zeta_o$$

$$\frac{\partial \zeta}{\partial \theta_o} = - \frac{\sin \zeta_o}{\sin \Delta}$$

$$\frac{\partial \zeta}{\partial \varphi_o} = - \frac{\sin \theta_o \cos \zeta_o}{\sin \Delta}$$

Given arrival time and/or dt/dΔ-azimuth data for a seismic event and a preliminary location, then Eqs. (I-1) and (I-2) provide us with a (generally overdetermined) system of linear algebraic equations to be solved for the desired changes in the hypocentral coordinates. Written in matrix form

$$\widetilde{A} \, \overline{x} = \overline{b} \tag{I-3}$$

where $\widetilde{A}$ is a matrix of the partial derivatives appearing in Eqs. (1-1) and (1-2) and has the form

$$
\widetilde{A} = \begin{bmatrix}
1/\sigma_i & \dfrac{\partial t_i}{\partial \Theta_o}\Big/\sigma_i & \dfrac{\partial t_i}{\partial \varphi_o}\Big/\sigma_i & \dfrac{\partial t_i}{\partial h_o}\Big/\sigma_i \\
& & & \\
\cdot & \cdot & \cdot & \cdot \\
\cdot & \cdot & \cdot & \cdot \\
\cdot & \cdot & \cdot & \cdot \\
0 & \dfrac{\partial p_{xj}}{\partial \Theta_o}\Big/\sigma_j & \dfrac{\partial p_{xj}}{\partial \varphi_o}\Big/\sigma_j & \dfrac{\partial p_{xj}}{\partial h_o}\Big/\sigma_j \\
& & & \\
0 & \dfrac{\partial p_{yj}}{\partial \Theta_o}\Big/\sigma_j & \dfrac{\partial p_{yj}}{\partial \varphi_o}\Big/\sigma_j & \dfrac{\partial p_{yj}}{\partial h_o}\Big/\sigma_j \\
& & & \\
\cdot & \cdot & \cdot & \cdot \\
\cdot & \cdot & \cdot & \cdot \\
\cdot & \cdot & \cdot & \cdot
\end{bmatrix}
\begin{array}{l}
\longleftarrow \text{arrival} \\
\quad\text{time} \\
\quad\text{datum} \\
\\
\\
\\
\Big\} \longleftarrow \text{slowness} \\
\qquad\text{datum}
\end{array}
$$

Notice that we have weighted each equation inversely with the estimated error σ for the corresponding datum. $\overline{x}$ is a column vector of the desired changes in the hypocentral coordinates:

$$
\overline{x} = \begin{bmatrix}
\delta t_o \\
\delta \Theta_o \\
\delta \varphi_o \\
\delta h_o
\end{bmatrix}
$$

$\overline{b}$ is a column vector of the residuals between the observed data and the values calculated for the trial hypocenter (again weighted inversely by the estimated errors):

$$
\overline{b} = \begin{bmatrix}
\delta t_i / \sigma_i \\
\cdot \\
\cdot \\
\cdot \\
\delta p_{xj}/\sigma_j \\
\delta p_{yj}/\sigma_j \\
\cdot \\
\cdot \\
\cdot
\end{bmatrix}
$$

7

The square of the modulus of $\overline{b}$ is the conventional measure of goodness of fit χ^2:

$$\chi^2 = \overline{b}^T \overline{b}$$

(T indicates transposition). (It should be emphasized that we are taking care not to interpret χ^2 too literally in terms of probabilities. Standard tables of the χ^2 distribution are based upon the assumption of independent, normally distributed errors which, as mentioned above, does not apply here. We use χ^2 merely as a rough estimate of whether the errors are about the size we expected them to be.) Since the system of Eqs. (I-3) is overdetermined, it cannot be solved exactly and we seek instead the solution which minimizes $[\widetilde{A}\,\overline{x} - \overline{b}]^T [\widetilde{A}\,\overline{x} - \overline{b}]$, which is the solution to the even-determined system

$$\widetilde{A}^T \widetilde{A}\,\overline{x} = \widetilde{A}^T \overline{b} \quad . \tag{I-4}$$

Furthermore, since Eqs. (I-3) are merely linearized approximations, they must be solved iteratively, each time with the revised hypocentral parameters, until these parameters cease to change.

To estimate the uncertainty in the final location, we need to know the effect upon the data residuals of possible changes in the hypocentral parameters. This problem may be analyzed conveniently in terms of the "shifted eigenvalue problem" for nonsquare matrices[3,4]:

$$\widetilde{A}\widetilde{V} = \widetilde{\Lambda}\widetilde{U}$$
$$\widetilde{A}^T \widetilde{U} = \widetilde{\Lambda}\widetilde{V} \tag{I-5}$$

where $\widetilde{U}$ and $\widetilde{V}$ are matrices whose columns are eigenvectors, and $\widetilde{\Lambda}$ is a diagonal matrix whose elements are eigenvalues. The eigenvectors are guaranteed to be orthogonal to each other, and are assumed to be normalized to unit length. From Eq. (I-5) we see that

$$\widetilde{A}^T \widetilde{A}\widetilde{V} = \widetilde{\Lambda}^2 \widetilde{V}$$

so that $\widetilde{V}$ and $\widetilde{\Lambda}$ may be calculated using conventional eigenvalue-eigenvector programs and the square matrix $\widetilde{A}^T \widetilde{A}$ appearing in Eq. (I-4). Now, from the orthonormality of the eigenvectors, it follows that $\widetilde{A}$ can be factored as

$$\widetilde{A} = \widetilde{U}\widetilde{\Lambda}\widetilde{V}^T \quad .$$

If we express a hypocenter perturbation $\overline{x}$ in terms of the eigenvectors

$$\overline{x} = \widetilde{V}\,\overline{y}$$

then the corresponding change $\overline{b}$ in the residual vector is

$$\overline{b} = \widetilde{A}\,\overline{x} = \widetilde{U}\widetilde{\Lambda}\,\overline{y} \quad . \tag{I-6}$$

This change is orthogonal to the error vector $\overline{b}_o$ corresponding to the best-fit location since, by Eq. (I-4), convergence of the iterative process implies $\overline{b}_o$ is orthogonal to the columns of $\widetilde{A}$. Therefore, the modulus of $\overline{b}$ gives the increase in χ^2.

Equation (I-6) says that a change of the hypocentral parameters in the direction of an eigenvector $\overline{v}_i$ and of length $1/\lambda_i$ will increase χ^2 by unity. Thus, the eigenvectors and eigenvalues completely specify the region of the four-dimensional space of location and origin time which will satisfy the data within any desired accuracy. Quality information of this sort is indispensable to the proper interpretation of any calculated hypocenter. Particularly for small events, the

resolut on of the available data is often so poor that a calculated location without supplementary inform tion on its uniqueness may be worse than useless.

B. R. Julian

D   FORTRAN SYSTEM MODIFICATIONS

The Fortran system for the two PDP-7 computers has been modified to take advantage of recently installed floating-point hardware. Most of the programs used at this facility show a marked improvement in calculation speed. Measurements taken on a few programs with limited input/output showed improvement by about a factor-of-5. Measurements on some representative actual Fortran routines showed: arithmetic calculations 5 times faster, trigonometric functions about 13 times faster, and exponential functions 17 times faster.

P. A. Neilson

REFERENCES

1. E. A. Flinn, "Confidence Regions and Error Determinations for Seismic Event Location," Rev. Geophys. 3, 157-185 (1965).

2. B. A. Bolt, "The Revision of Earthquake Epicenters, Focal Depths, and Origin-Times Using a High-Speed Computer," Geophys. J. 3, 434-440 (1960).

3. C. Lanczos, Linear Differential Operators (Van Nostrand, London, 1961).

4. R. A. Wiggins, "The General Linear Inverse Problem: Implications of Surface Waves and Free Oscillations for Earth Structure," Rev. Geophys. Space Phys. 10, 251-285 (1972).
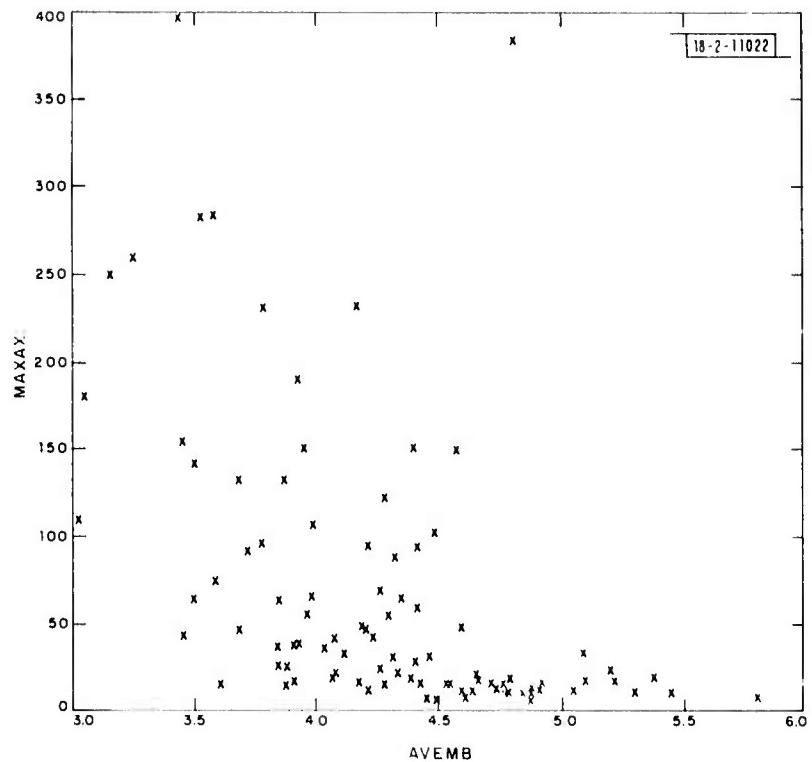
Fig. I-1. Length (in km) of largest principal semiaxis of epicenter error ellipse (MAXAX2) vs event m_b (AVEMB) for ISM events during three-day time period.

II. NORSAR

A. SHORT-PERIOD CHARACTERISTICS OF NORSAR

In the last SATS (31 December 1972, DDC AD-757560), examples of amplitude variations across NORSAR from teleseismic events illustrated the complexity of scattering produced by deep structure under NORSAR. The measured amplitudes consisted of peak-to-peak motion in nanos/second measured on the center sensor trace of each subarray.

One of the puzzling features of the data was that inconsistent patterns across NORSAR were obtained for two closely located presumed explosions in Eastern Kazakh. This result implied that the amplitude patterns were controlled not by scattering of waves by structure under NORSAR, but rather by source and transmission path effects further removed from NORSAR. This was contrary to results obtained for two deep Hindu Kush events with close epicenters. Although the NOS depths for the Hindu Kush events differ by 80 km, very similar amplitude patterns were produced across NORSAR. These data suggested that the deep structure under NORSAR was the dominant factor which controls the amplitude pattern across the array.

These contradictory results have been resolved by a more-detailed frequency domain analysis of the data. The main conclusion is that the amplitude patterns across NORSAR are strongly frequency dependent, and that measurements of nanos/second from records give consistent amplitude patterns only for source functions with similar spectra and phase. Events from the same regions with dissimilar spectral peaks may have very different amplitude patterns in nanos/second across NORSAR. This scattering effect is accentuated at NORSAR by the crustal geology. The shield under NORSAR has a very high Q which transmits a wide band of frequencies to the sensors.

TABLE II-1				
NOS DATA FOR TWO PRESUMED SOVIET EXPLOSIONS				
Event	Date (1971)	Origin Time (GMT)	Location	Magnitude (m_b)
1	6 June	04:02:57.1	50.0°N 77.8°E	5.5
2	30 June	03:56:57.2	50.0°N 79.1°E	5.4

As an example, we present here the amplitude patterns of two presumed explosions in Eastern Kazakh which have clearly unequal source functions. The NOS data for the events are given in Table II-1.

Figures II-1 and II-2 show the center subarray sensors and steered beams at NORSAR for events 1 and 2, respectively. Event 1 was chosen because it has an impulsive high-frequency beam with a period of ~0.4 sec. Event 2 has a more-complex beam with an apparent period of ~1.0 sec. The spectra of these two beams are displayed in Fig. II-3. The beam spectrum of event 1 is nearly flat from 1 to 3 Hz, whereas the spectrum of event 2 peaks at 1 Hz with a pronounced notch at ~1.7 Hz, due to the interference seen on the beam in Fig. II-2.

Event 1 can be used to calibrate the array if we assume that the beam is a good estimate of the source incident to the crustal structure under NORSAR. The spectrum of each sensor waveform for this event will indicate the spectral response of the structure under NORSAR to Eastern

Kazakh events. In Fig. II-4, the spectral responses of the individual waveforms of event 1 are plotted at frequencies of 1, 2, and 3 Hz. These spectra were computed using 20 sec of cosine-tapered data. On the right-hand side of the figure are the spectral values of the steered beam.

Figure II-4 clearly shows that the array response varies from 1 to 2 Hz. Sensors 16, 17 and 18, for example, have nearly equal responses at 1 Hz, whereas at 2 Hz, sensor 17 has a response well below that of 16 or 18. This explains the apparent inconsistency in waveform shapes at these sensors for events 1 and 2. In Fig. II-1, the waveform amplitudes at sensors 16, 17, and 18 match the 2-Hz pattern at the same sensors in Fig. II-4. However, in Fig. II-2 the same sensors have nearly equal amplitudes, and match the 1-Hz pattern in Fig. II-4. Even the high frequency content of sensors 16 and 18, which is absent on sensor 17 in Fig. II-2, is predicted by the array response in Fig. II-4.

In order to investigate the consistency of crustal scattering in more detail, least-squares time-domain filters were computed for shaping the beam of each event to the individual sensor waveform. This removes the source from each waveform and isolates the scattering received at each sensor. These filters contain smoothed phase and amplitude information in the frequency domain. Figures II-5 and II-6 show the computed filters for events 1 and 2, respectively. In spite of the different source spectra of the two events, the two sets of filters are very similar in shape and amplitude.

In Fig. II-7, some of the more coherent pairs of filters for the two events are shown aligned in time. The filters appear to be most coherent in the first one or two seconds of time, although in some cases coherent bursts arrive later in time. Coherence in the time domain carries over into the frequency domain. In Fig. II-8, the spectra of the two filters for sensor 2 are superposed. The notch in amplitude at 2 Hz in both spectra indicates that the scattering recorded at this sensor is probably a multipath phenomenon.

Attempts are being made to examine the spectral amplitudes at NORSAR from events of various azimuth and distance and relate these to crustal and Moho structure.

<div align="right">C. W. Frasier</div>

B. NORSAR ARRAY MISLOCATIONS

A sizable data base of good-quality well-recorded events at NORSAR is being used to obtain values for the array epicenter location errors, as well as the subarray time anomalies. While the complete picture of the time anomalies is not yet available, we have obtained a good picture of the epicenter mislocations that NORSAR would produce without using any station corrections. The time delays were obtained from the event processor at NORSAR and were corrected to agree with visual recordings. A plane wave was fitted, in a least-squares sense, to each set of delay times. The resulting measurements of velocity and azimuth, and therefore latitude and longitude, were plotted against the true epicenter or velocity and azimuth obtained from the standard J-B tables. The resulting plots show effects that were not widely observed at LASA, yet seem to be prevalent at NORSAR.

On first analysis of the array diagram in Fig. II-9 (a polar plot with $dT/d\Delta$ as the radial component), there is no one overriding trend as was observed at LASA. In this figure, the slowness and azimuth of the true epicenters reported by NOS are represented by the arrowheads and plotted at the slowness values given from the J-B tables. The array measurements of azimuth and slowness are plotted as the tails of the arrows. Only P-wave data were used. It is difficult

to see any universal bias to the arrows in Fig. II-9. This was not the case at LASA,[1] where there appeared to be a constant mislocation term. Figure II-10 is a projection of the coastal outlines into slowness and azimuth and will help in interpreting the array diagram. On a large projection of the array diagram, it is evident that there are a number of regions where the mislocation vector will change rapidly over small changes in azimuth or slowness. These areas are not usually the same areas of rapid change observed at LASA.

When the mislocation vectors are plotted on a geographic map, it is possible to see the areas of rapid change more clearly. Figure II-11, for example, shows how the location error changes as the epicenters move from western United States to central South America. Over this region, the azimuthal constituent of the location error varies rapidly while the slowness values of these events decrease right into the core. What we are seeing here is an array location error changing sign and passing through a zero-location error point around Central America. This is quite clear when viewed in Fig. II-9 at the azimuth of 270°. A small set of events in the Central America region shows still another interesting effect. These events from the Oaxaca district of Mexico, indicated by the box in Fig. II-11, are actually quite close to each other and yet with only a slight shift in epicenter, less than 75 km, the array locations are shifted by as much as 700 km. One can draw a line through this region which will clearly separate the epicenters into two distinct anomalies, yet each epicenter will be within a few tens of kilometers of the line. This feature clearly seems to be source or path related, whereas the overall trend within Fig. II-11 could possibly be due to near array effects.

Another interesting area to note is in western Asia around the China, Russia, Afghanistan borders (Fig. II-12). In this region, where the seismic zones of Hindu Kush and northern Sinkiang meet, the azimuth from NORSAR will change by only a few degrees, yet the epicenter location error will almost completely reverse itself. It is supposed that this feature is also primarily a source/path effect.

As more processing of the data occurs, it is expected that many more interesting features will emerge. Still to be analyzed in detail however are the individual subarray anomalies.

<div align="right">R. M. Sheppard</div>

C. ANALYSIS OF 40-SEC-PERIOD RAYLEIGH-WAVE CODA AT NORSAR

The occasional long persistence of Rayleigh-wave coda can make it difficult to apply the M_s-m_b discriminant to subsequent signals received at a seismic station. Previous work[2,3] at LASA revealed the contribution of multipath energy to this coda and the desirability of studying 40-sec energy which should suffer less multipathing.

A similar analysis of the 40-sec-period Rayleigh-wave coda is being done at NORSAR. Some preliminary results are now presented. A total of 16 events, each with $m_b \geqslant 5.5$, located at various azimuths and distances from NORSAR, have been selected. There were no events occurring close in time to the chosen events, according to the NOS monthly summary reports and the NORSAR bulletin. The high-resolution wavenumber analysis method was modified so as to pre-filter the NORSAR LPZ seismometer data in a manner similar to that done previously at LASA.[2] The results of the analysis for the 12 June 1972 Aleutian Island event are shown in Figs. II-13(a-d) and II-14(a-d).

In Fig. II-13(a) we see that, during the first 200 sec following the onset time of the 40-sec period group, the peak power occurs at an azimuth of 0° and with a phase velocity corresponding

approximately to that of a fundamental-mode Rayleigh wave. Thus, during this time, the group arrives at NORSAR from very close to the true azimuth of this event at NORSAR, which is 358.5°. In Figs. II-13(b) and (c), there are very clear indications of multipath propagation of 40-sec period groups at NORSAR. An effort is under way to try to identify the propagation paths for the various phases which are being detected in the coda at NORSAR.

Preliminary results at NORSAR seem to indicate that the coda power level decreases more rapidly than that found at LASA. For example, the data in Figs. II-13 and II-14 show that the power level decreases by 30 dB after 20 minutes. This is about 10 dB better than the average value found at LASA,[2] which indicates that NORSAR may have an important role to play in a network for detecting interfering Rayleigh waves.

<div align="right">

J. Capon
H. Bungum*

</div>

REFERENCES

1. D. Davies and R. M. Sheppard, "Lateral Heterogeneity in the Earth's Mantle," Nature 239, 318-323 (1972), DDC AD-758942.

2. J. Capon and J. F. Evernden, "Detection of Interfering Rayleigh Waves at LASA," Bull. Seismol. Soc. Am. 61, 807-849 (1971), DDC AD-734105.

3. J. Capon, "Analysis of Rayleigh-Wave Multipath Propagation at LASA," Bull. Seismol. Soc. Am. 60, 1701-1731 (1970), DDC AD-716084.

---

* NORSAR Data Centre, Kjeller, Oslo.
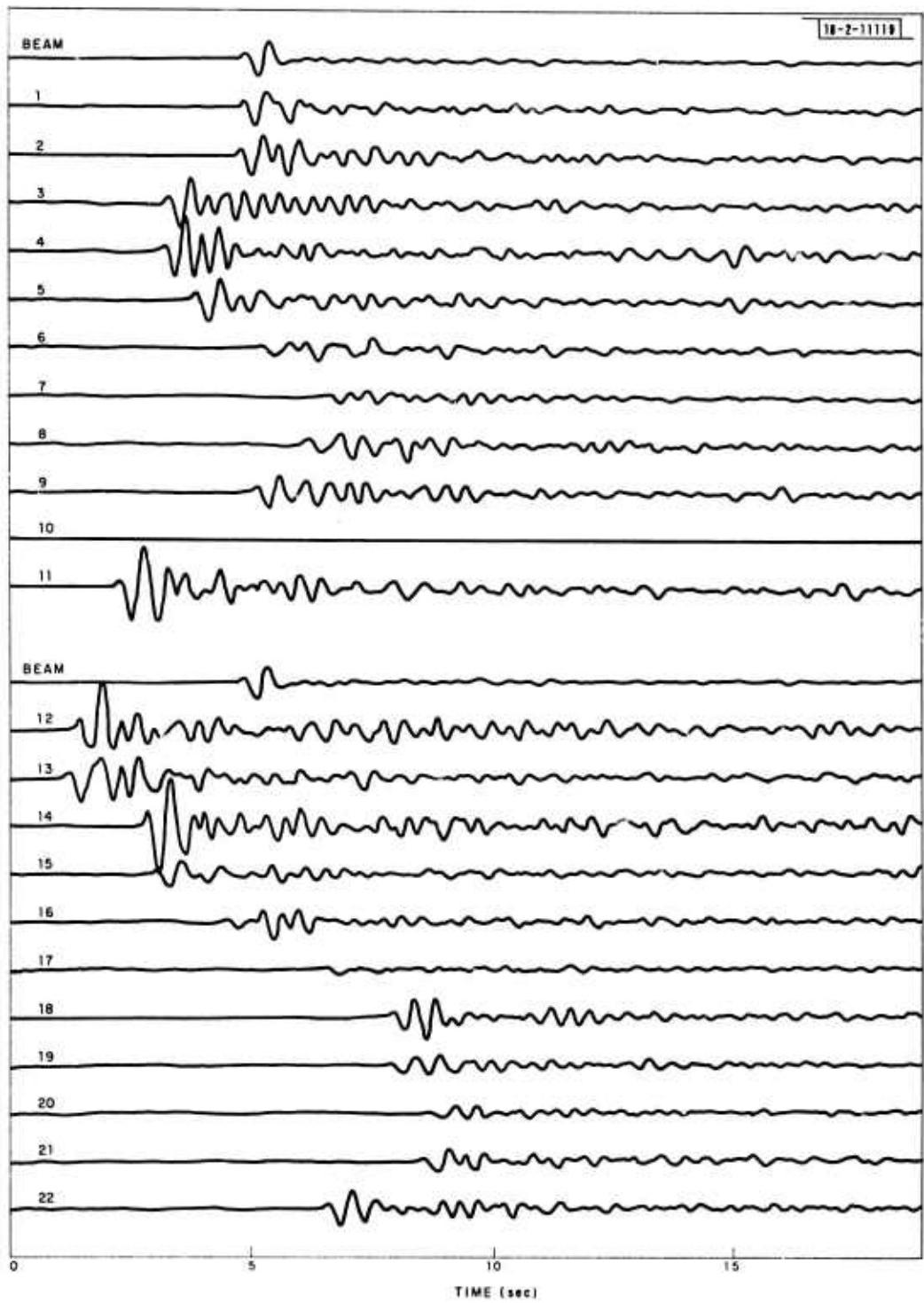
Fig. II-1. NORSAR data for event 1. Sensors 1 to 22 correspond to center subarray sensors 1A0, 1B0, ..., 7B0, 1C0, ..., 14C0. Also displayed above sensors 1 and 12 is steered beam.
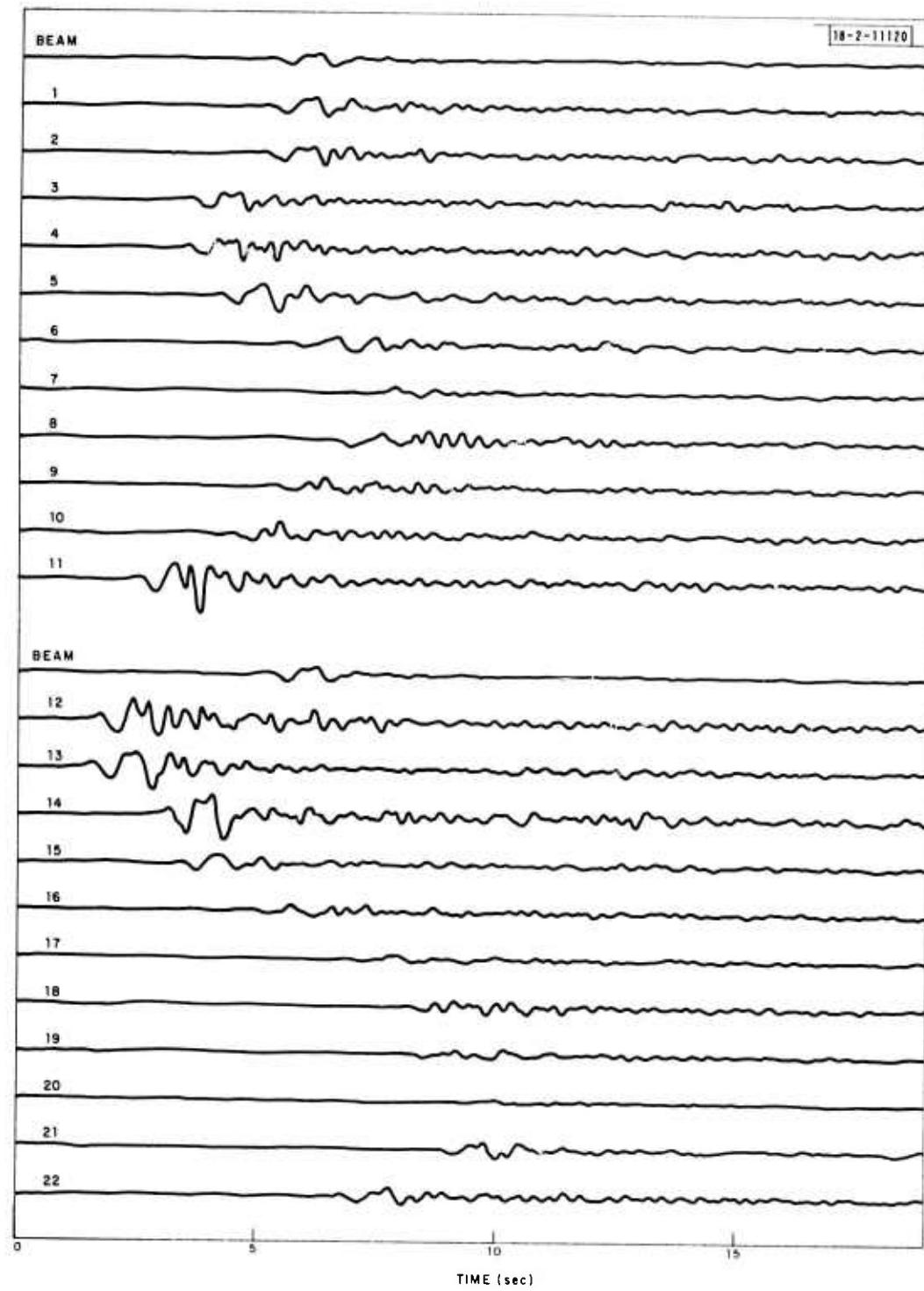
Fig. II-2.   NORSAR data for event 2.   Sensors 1 to 22 are displayed with steered beam.
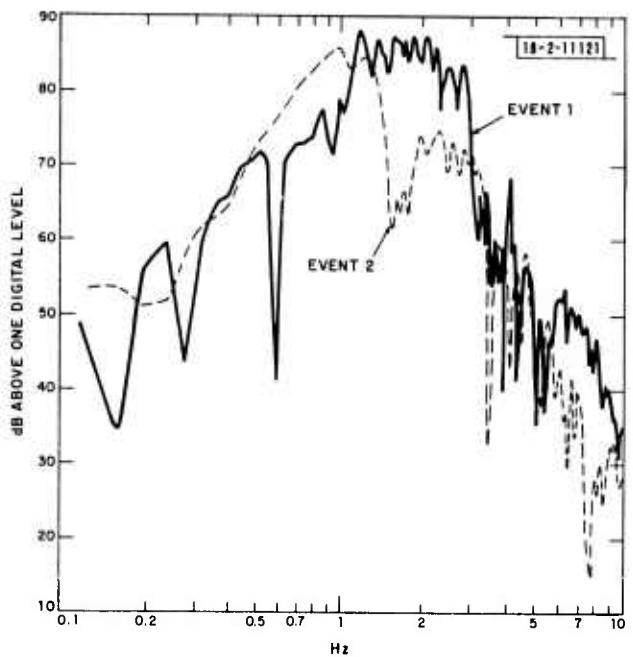
Fig. II-3. Uncorrected amplitude spectra of events 1 and 2 in decibels above one digital level. Instrument response is approximately flat in ground motion (n/sec) from 1 to 5 Hz.

17
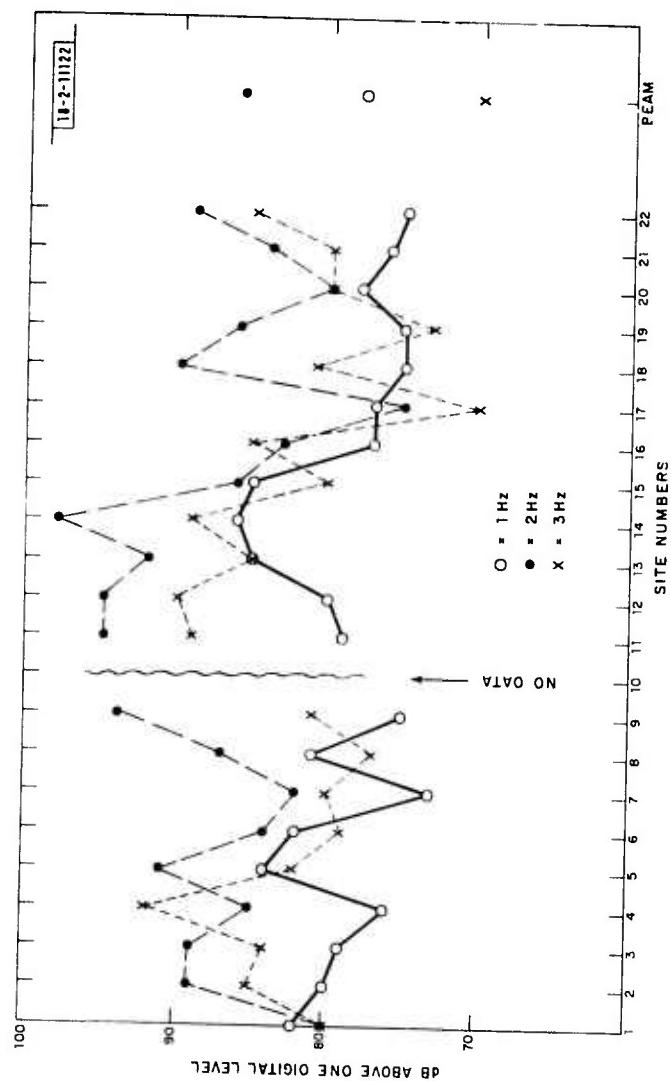
Fig. II-4. Spectral response of center sensors to event 1 at 1, 2, and 3 Hz in decibels above one digital level.

18
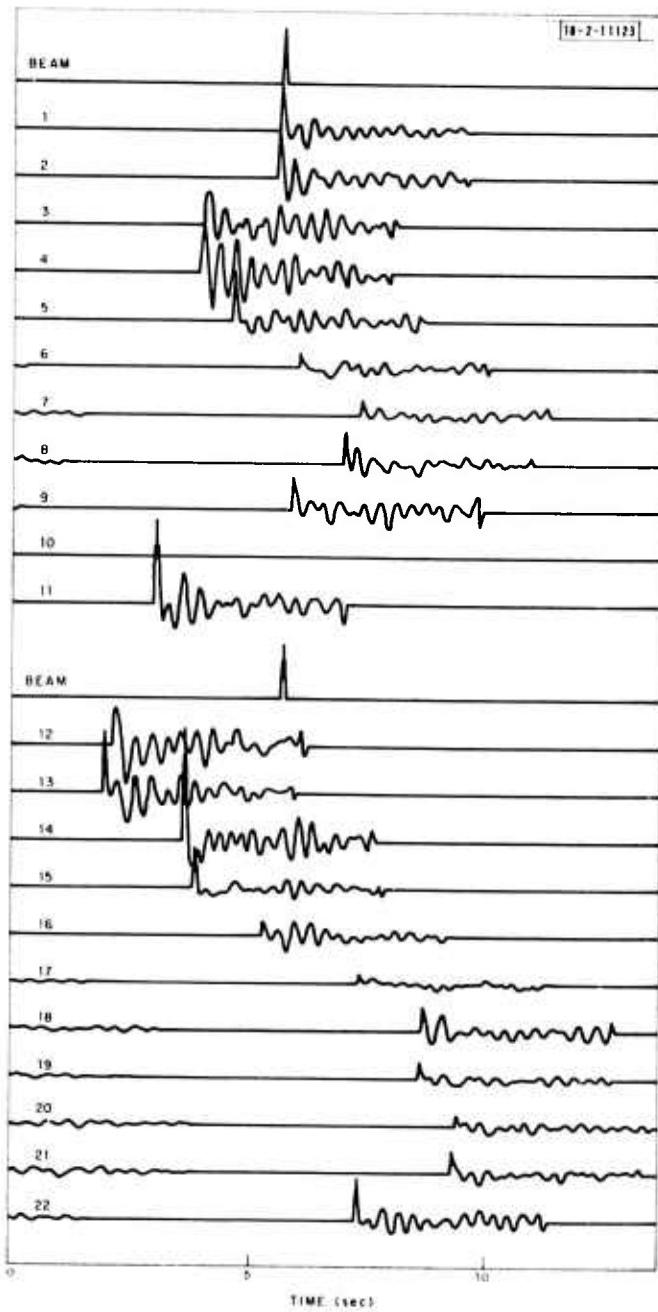
Fig. II-5.   Time-domain filters to shape beam of event 1 to each of center sensor waveforms and beam shown in Fig. II-1.   Spike on beam trace has amplitude 1.
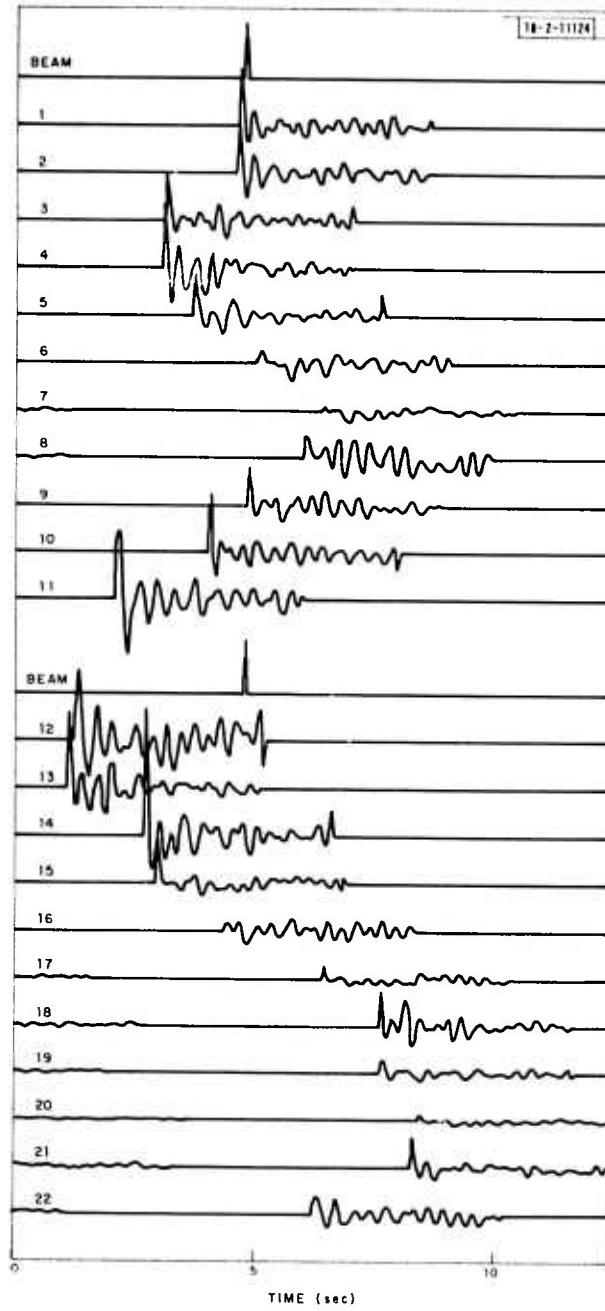
Fig. II-6.   Time-domain filters to shape beam of event 2 to each of center sensor waveforms and beam shown in Fig. II-2.   Spike on beam trace has amplitude 1.

18 - 2 -11125

SENSOR 2 — EVENT 1
— EVENT 2

SENSOR 6

1.0

SENSOR 14

SENSOR 16

0 1 2 3 4

SEC
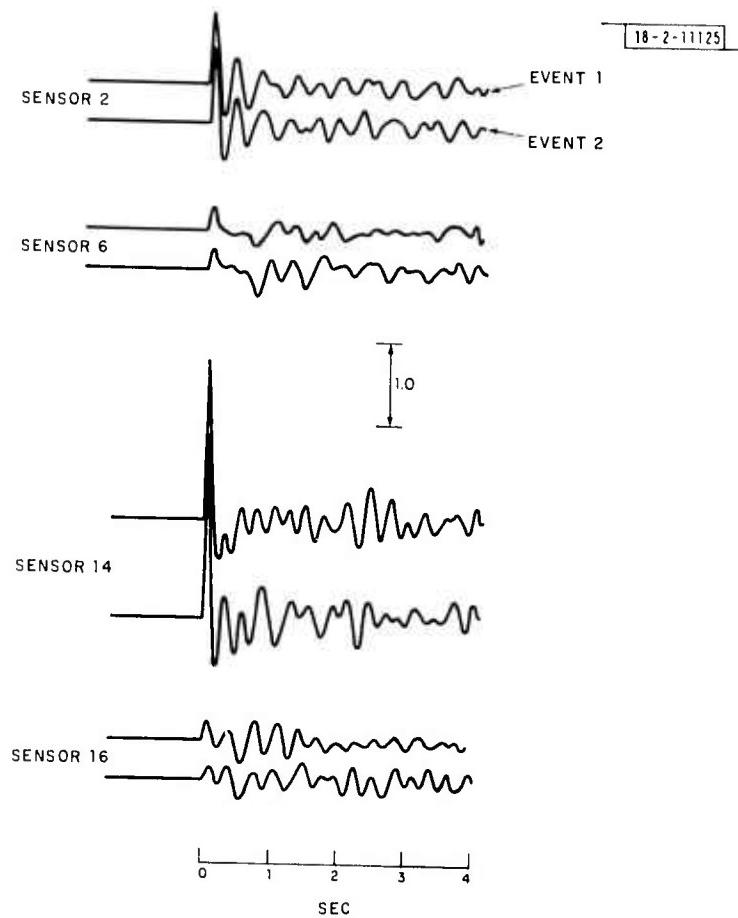
Fig. II-7. Comparison of some coherent filters for events 1 and 2 at 4 sensors.

18 - 2 -11126

EVENT 1

EVENT 2
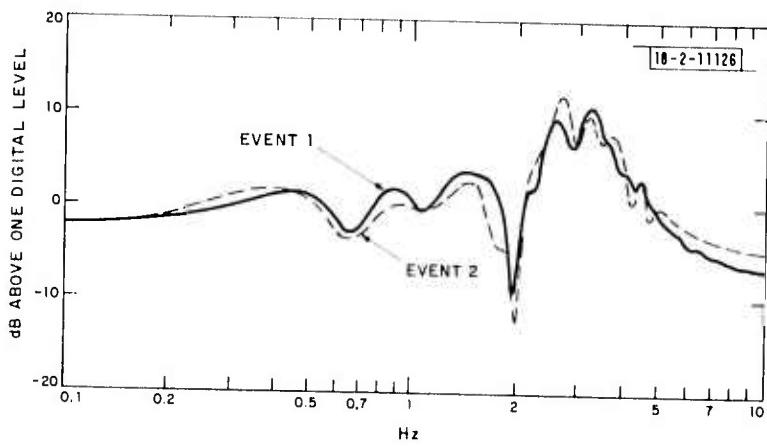
Fig. II-8. Superposed spectra of filters for sensor 2, shown in Fig. II-7. Vertical scale is decibels above spectrum of spike of unit height.

21
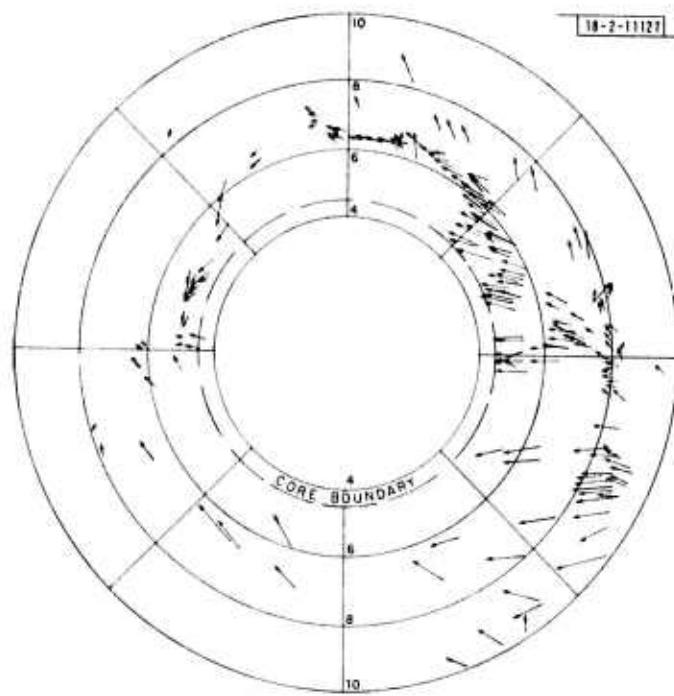
Fig. II-9.   NORSAR array diagram for P-waves.
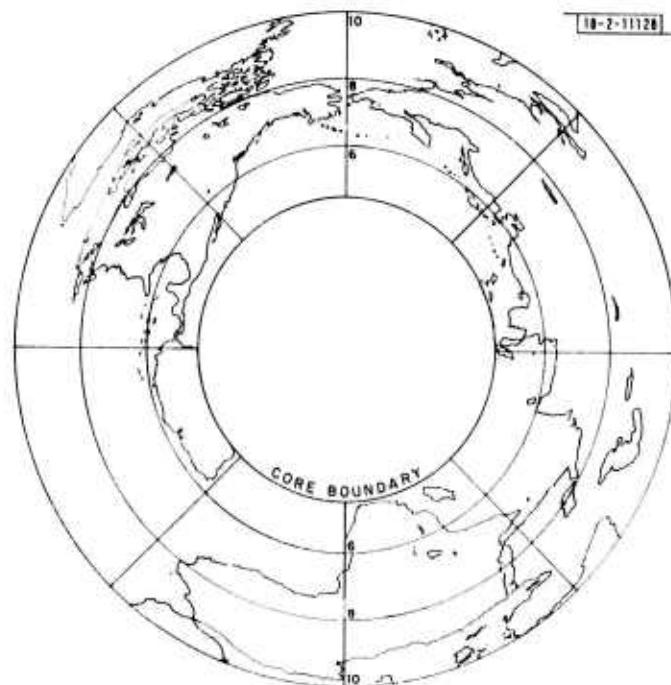
Fig. II-10.   Coastal outlines in slowness projection from NORSAR.
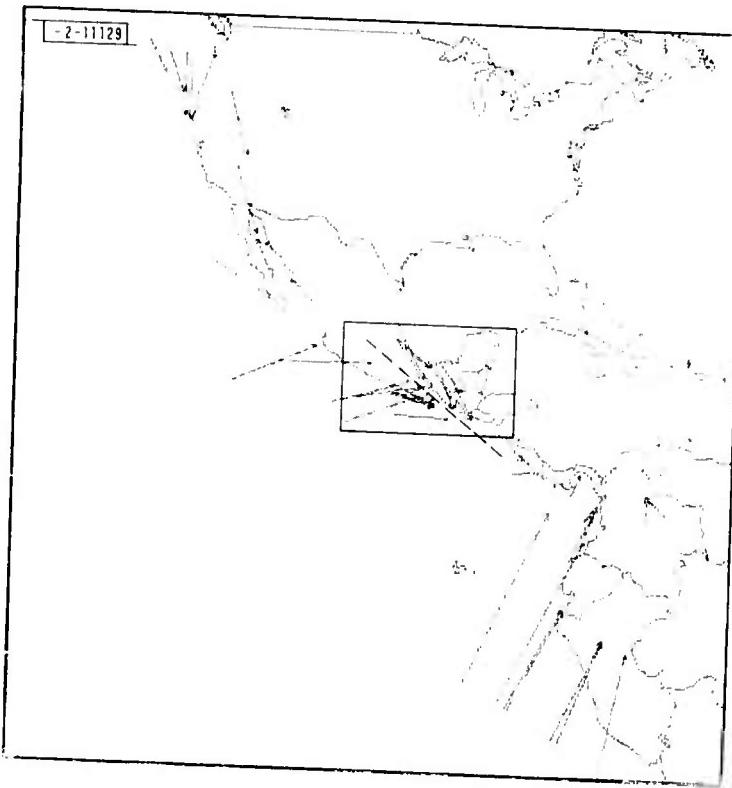
Fig. II-11. NORSAR location errors in Americas.
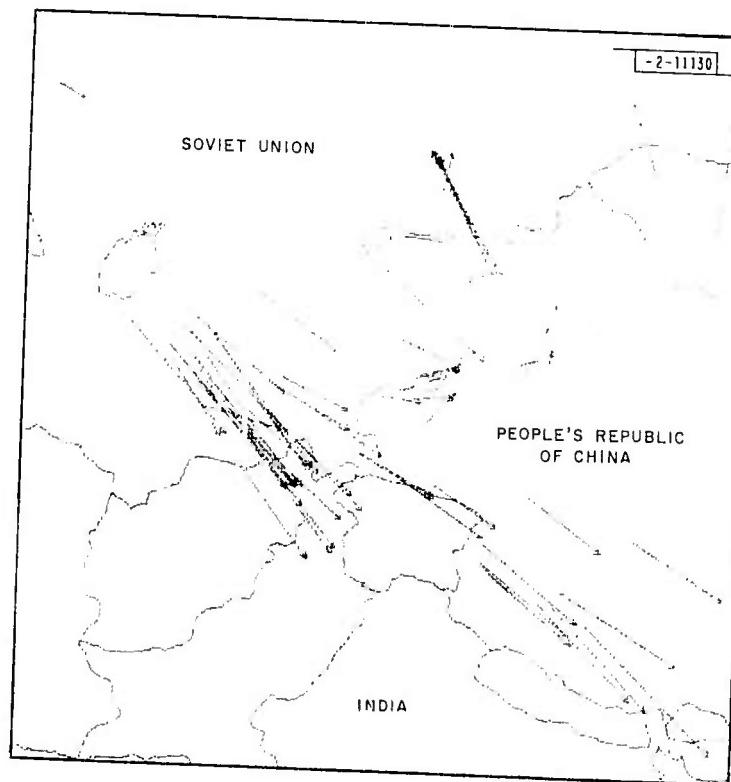
Fig. II-12. NORSAR location errors in Central Asia.
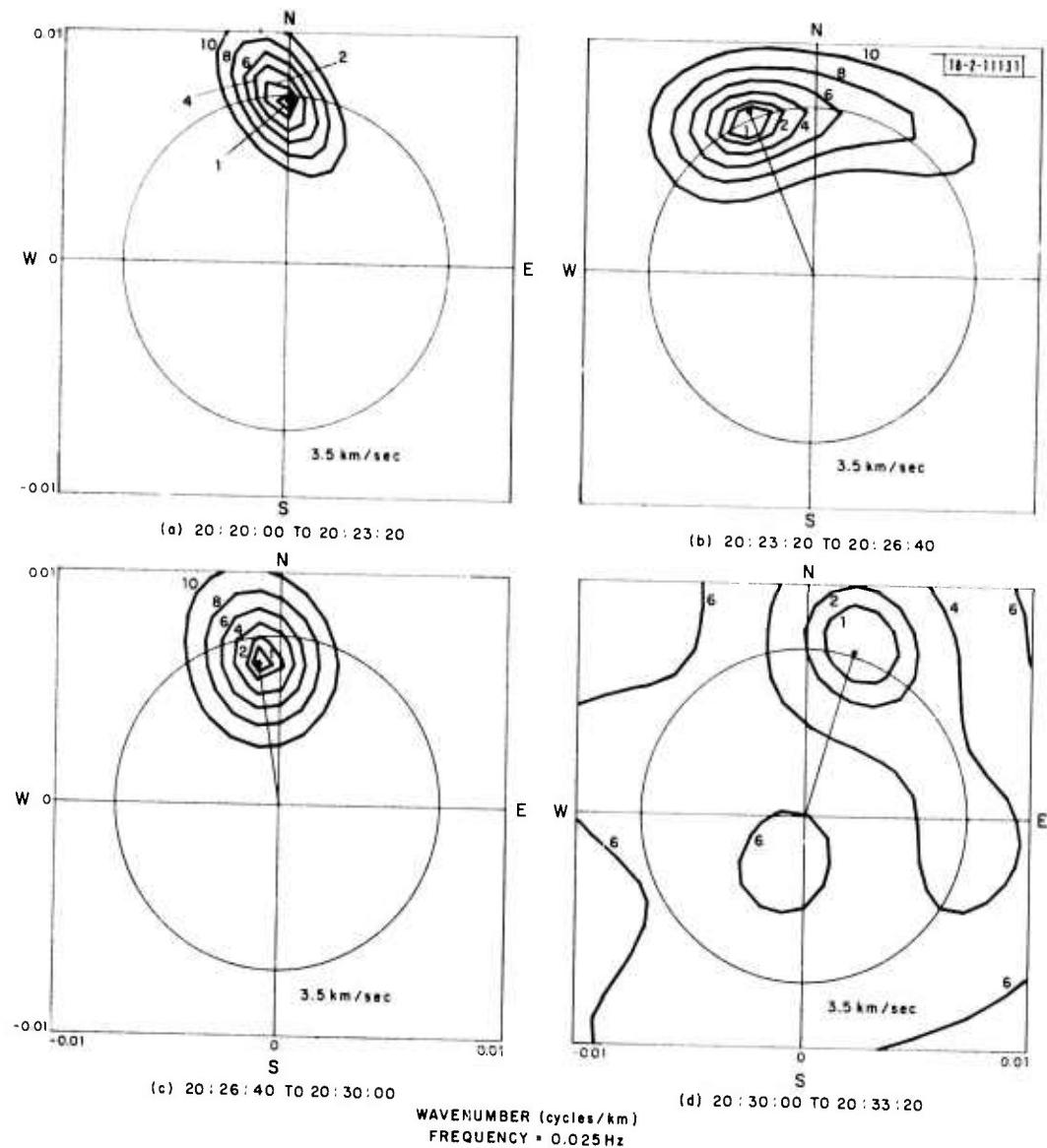
Fig. II-13(a-d). High-resolution frequency-wavenumber spectra for prefiltered waveforms of 12 June 1972 Aleutian Islands event measured over four consecutive nonoverlapping 200-sec intervals starting at onset time of Rayleigh wave.
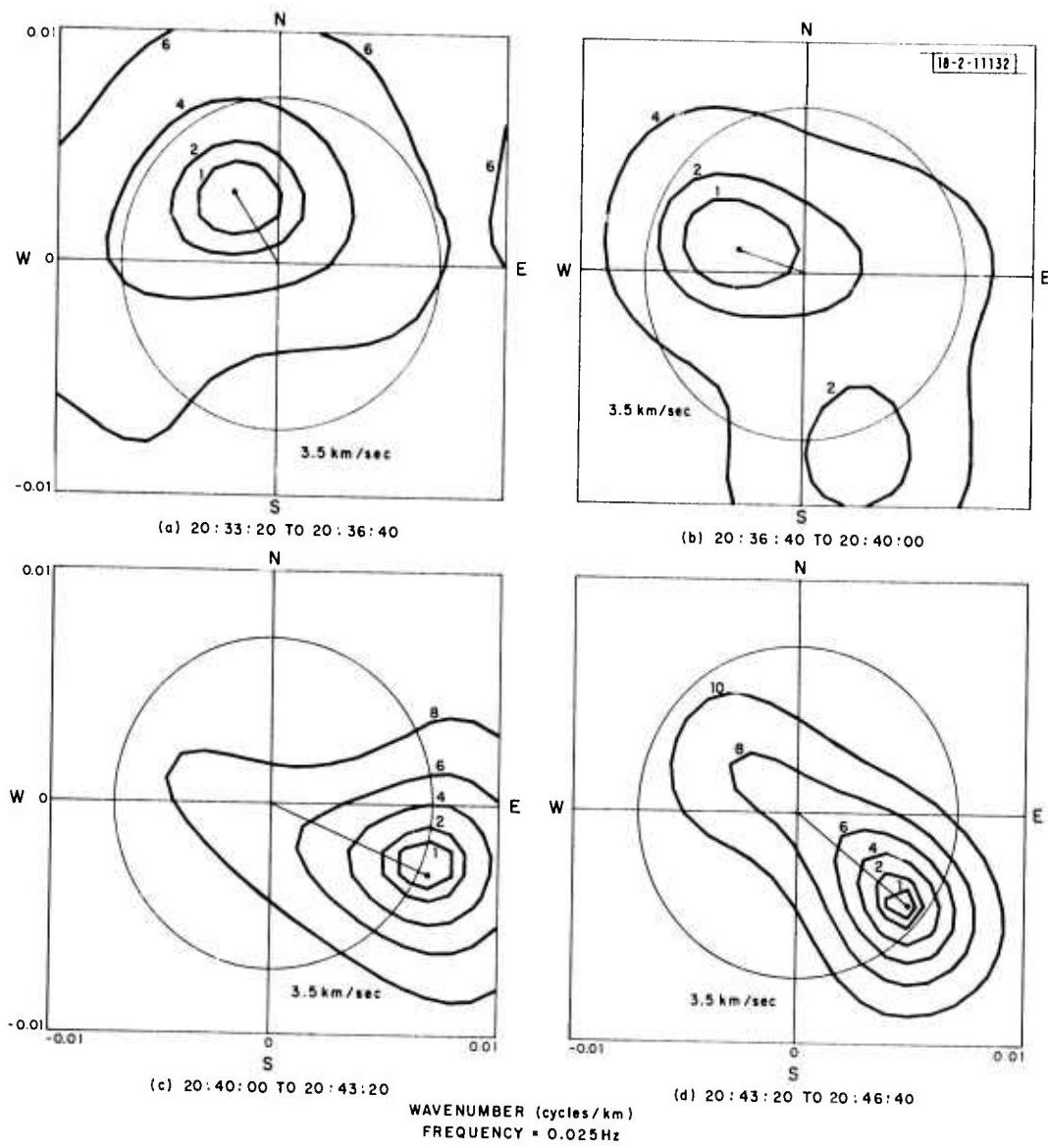
Fig. II-14(a-d). High-resolution frequency-wavenumber spectra for prefiltered waveforms of 12 June 1972 Aleutian Islands event measured over four consecutive nonoverlapping 200-sec intervals starting 800 sec after onset time of Rayleigh wave.

III. LATERAL HETEROGENEITY

A. PREDICTING RAYLEIGH-WAVE-PROPAGATION BEHAVIOR FROM GEOLOGICAL AND GEOPHYSICAL DATA

In the SATS dated 30 June 1972 (DDC AD-748304), preliminary results were given of an experiment aimed at using ray tracing to explain in detail multipath propagation and lateral refraction of Rayleigh waves. The results of that experiment, based on a very crude model containing only oceans and continents, compared well with observed data and have encouraged us to undertake experiments with more complicated models to find out the degree of detail with which surface wave propagation on the real earth may be predicted.

There are several ways in which a detailed understanding of surface wave propagation would be of value in the seismic discrimination problem. Surface wave magnitude (M_s) measurements are affected by regional differences in dispersion and, probably more severely, by geometric spreading caused by lateral refraction. Accurate path corrections for these effects would make M_s measurements for small events more reliable. The same dispersion and spreading information would enable synthetic seismograms to be computed much more accurately than is now possible, and would thus improve our ability to detect small signals by matched filtering. Multi-pathing calculations would enable reliable associations to be made between observed signals and seismic events in cases of ambiguity, and thus are of great potential use in the interfering event problem.

We have chosen to deal with the western United States, because relevant surface wave data are available from LASA and because extensive geological and geophysical data on crust and upper mantle structure are available. The results discussed here apply to models incorporating information on crustal thickness (see Fig. III-1), upper mantle velocities, and crustal structure differences between geological provinces.

Figures III-2(a) through (d) show Rayleigh wave rays traced outward from LASA in such a model. These calculations may be compared with the observations reported by Landers in the last SATS (Fig. 1-19)[1] of azimuth anomalies at LASA for Rayleigh waves from the Nevada Test Site. At 10-sec periods, the waves arrived 10° to the west of the great circle azimuth, in nearly perfect agreement with the prediction of Fig. III-2(a). This anomaly is caused by refraction at the boundary of the Snake River Plain, in which the crust (consisting entirely of basalt) has very high seismic velocities. The observed azimuth anomaly disappears at about 20 sec, also in agreement with prediction [Fig. III-2(b)], but at longer periods the observed waves arrive to the east of the great circle, and no such effect is predicted [Figs. III-2(c) and (d)]. An attempt to resolve this discrepancy by raising the mantle velocity in the Colorado Plateau proved unsuccessful.

Thus, on the basis of these limited data, we have predicted the short-period behavior of Rayleigh waves quite well, and discovered that our knowledge of the Colorado Plateau-Basin and Range boundary is inadequate in some yet unknown respect. Current work is aimed at refining the model (e.g., incorporating sediment thicknesses) and acquiring more data against which to test it.

B. R. Julian

B. BODY-WAVE MULTIPATHING – EVIDENCE FROM TIME-DOMAIN ANALYSIS

In the last SATS,[1] Capon and I presented evidence which indicated that waves from a region in South America followed paths from source to receiver which were dependent on frequency.

We four·l in particular that frequencies less than 1 Hz followed a path significantly different in azimuth from that followed by frequencies greater than 1 Hz.

A very simple and large earthquake in the Hindu Kush (20 January 1972, depth = 220 km, m_b = 6.0) has revealed multipathing which is visible even on the unprocessed seismometer outputs. Figure III-3 shows 6 subarray sums for short-period P-waves from across the whole aperture of the array. It is clear that the signal consists of a primary pulse, followed by later activity among which a secondary pulse is prominent and has been aligned in the figure. Alignment of the secondary pulse however yields, as is obvious from Fig. III-3, a different arrival vector from alignment of the primary pulse.

TABLE III-1		
WAVE PARAMETERS FOR THE TWO HINDU KUSH PHASES		
Phase	dT/dΔ (sec/deg)	Azimuth (deg)
1	4.07	357.4
2	4.28	358.2
Phase 2 arrives at A0, approximately 2.1 sec after phase 1.		

The two phases clearly arrive with different values of $dT/d\Delta$, although the azimuths along which they arrive are not significantly different. Note that the determinations of wave parameters for Table III-1 were made by least-squares fitting of a plane wave to the raw arrival times. No subarray corrections were applied. For this reason, although the data in Table III-1 represent estimates relatively free of personal prejudice, the absolute values of $dT/d\Delta$ and azimuth should not be taken seriously, as they are subject to bias from structure beneath the array.

It is clear that the $dT/d\Delta$ values are too significantly different for us to consider the possibility that this is a source phenomenon, such as a double rupture. Examination of the single-pulsed PKKP at LASA confirms this. Nor can it be easily ascribed to the region under LASA. If, for instance, it were a P-to-S conversion phenomenon,[1] we would expect that the delays between phases 1 and 2, representing sediment thicknesses, would be random. This they are not. In Fig. III-4 we plot time residuals to phase 2 against time residuals to phase 1 for each subarray, and it is clear that they are strongly correlated. This implies that the two waves have experienced the same perturbations on a plane wave front on approaching LASA, and therefore that the effect is not locally generated.

Further powerful constraints on the location of the source of multipathing come from the time delay of 2 sec between the first and second pulse. Figure III-5 is a very schematic ray diagram. Returning from LASA are a pair of rays separated by an (exaggerated) angle intended to represent the $dT/d\Delta$ difference between the two pulses. Note that the second pulse has a larger $dT/d\Delta$, bottoms at a shallower depth, and therefore cannot be PcP. If the earth were laterally homogeneous and a sharp turn were introduced into ray paths only by a localized feature which did not affect the travel time along the path, to produce a 2-sec time differential it would be necessary for the two ray paths to run back until, within 600 km of the surface near source, one of the rays turned. This is one of the options sketched in Fig. III-5; another is that there

28

are sufficiently strong velocity gradients just above the core that there is triplication in the travel time curve. A variety of other explanations intermediate between these two extremes exists, but it should be clear that any complex structure beneath LASA (say, on the 650-km discontinuity), although it might be capable of generating multipaths, would not in any reasonable model yield time delays of 2 sec or more. I thus conclude that a complexity of earth structure exists back along the ray paths either in the deep mantle or beyond toward the source, such that at least two possible paths exist from source to receiver.

<div align="right">D. Davies</div>

C. AMPLITUDES OF P-WAVES THAT HAVE TRAVERSED THE DEEP MANTLE

We have studied the amplitudes of short-period P-waves in the distance range 90° to 105° and some rather striking features have emerged. A full account of this work is given in a paper now in press,[2] so we will simply outline the main conclusions.

Seismicity around the Pacific from New Guinea to Kermadec gives a rather good coverage at the distance 98° to 102° for azimuths from 235° to 275° from LASA. It is clear that events of the same body wave magnitude (NOS) do not necessarily have the same amplitude on an equi-distant contour. For instance, "visibility" to Santa Cruz is much inferior to visibility to points in Fiji and the Solomon Islands at the same distance. It is possible to eliminate effects under LASA fairly easily, but more attention must be paid to the possibility of source region effects. However, after careful consideration of the effect of a dipping slab, or a low Q zone, we have concluded that the source region cannot be the culprit either. We are thus left with propagation effects in the middle or deep mantle as the most likely cause. It is not immediately possible to distinguish between velocity and Q heterogeneity. The dimension of the anomaly at LASA is 10° of azimuth. This suggests some feature a few hundred kilometers across deep in the earth.

<div align="right">R. E. Needham
D. Davies</div>

D. ANALYSIS OF ARRAY DIAGRAM AT LASA

In the last SATS,[1] a discussion was presented on the representation of approach angle, or slowness, anomalies for P-wave signals at an array in slowness ($dT/d\Delta$, azimuth) space. Such a representation, known as an array diagram, involves the plotting of these anomalies as arrows. The tail represents the $dT/d\Delta$ and azimuth measured for the P-wave signal at the array, and the head represents the $dT/d\Delta$ and azimuth that would be obtained from the true (or, in this case, NOS) location and J-B tables. This approach has been used by Manchee and Weichert,[3] Vinnik and Nikolayev,[4] and by Davies and Sheppard[5] at LASA.

If the anomaly were caused by a plane-dipping interface directly under the array, the array diagram would consist of a set of error vectors whose magnitudes were all approximately the same and which all pointed in the direction of dip of the interface. Thus, the effect of a sloping interface can be obtained from the array diagram by fitting a constant vector to the error vectors in the diagram. These results were first pointed out by Manchee and Weichert.[3] Davies and Sheppard[5] pointed out that a smoothly varying distribution of arrows, all approximately of equal length and pointing in the same direction, would indicate a bias introduced beneath the array — not necessarily from a dipping interface but, for example, from a distribution or coating of delays that are not directionally independent.

The spatial rate of variation of the error vectors can at least formally be associated with heterogeneities at certain depths in the earth. The more rapid these spatial variations become,

the more distant from LASA the heterogeneities must be placed to explain the anomalies. The reason for this can be seen, qualitatively at least, on the basis of the separation of the ray paths from the various event epicenters to LASA. We now wish to give a more quantitative proof for this important result, since it forms the basis for an analysis of the array diagram. Suppose that the region under LASA can be divided into a series of sub-regions, each of which can be considered a horizontal disk extending between certain depths as shown in Fig. III-6. The outer boundaries of these disks are defined by the P-wave ray paths which have a dT/dΔ of about 10 sec/deg, as indicated in Fig. III-6. We consider first the topmost disk extending between 0 and 75 km. The effect of this region on the propagation of the P-waves can be obtained by considering the region to be approximated by a combination of a time delay coating, and a random medium. It was shown in the last SATS[1] that this approximation appears to be reasonably good for the earth structure under LASA. In addition, it was shown that LASA tends to average out the effects due to the laterally heterogeneous medium on the P-wave signals, so that the effect of the coating dominates. This coating produces an anomaly component which must be the same for all vectors in the array diagram, since it is located so close beneath the array that all P-wave ray paths must pass through it. Therefore, the effect of the coating may be obtained by determining the average of all the error vectors in the array diagram. It must be said as a caution that Fig. III-6, showing rays as straight lines, is clearly no more than a schematic representation intended to start discussion.

We now consider that the effect of the region in the 0- to 75-km range has been removed from the array diagram by subtracting the average of all the error vectors from each of these vectors. We now examine the disk in the 75- to 225-km depth range. The horizontal cross section of this disk, at a depth of about 150 km, is equal to about four times the area of the LASA aperture. It is now assumed that this disk can be divided into four regions, each of which can once again be approximated by a tandem combination of a coating and random medium. Since there are four such coatings, there will be four independent error vectors introduced in the array diagram. Each of these anomaly vectors is caused by an associated coating, since the effect of each of the random media is averaged out by LASA as indicated previously. In addition, each vector would be approximately constant over an area roughly equal to one-fourth of the total area of the array diagram. Thus, in order to evaluate each of these vectors, the array diagram is divided into four quadrants, and an average of the error vectors (with the average vector removed) is performed in each quadrant. Once again, we can consider that the effect of the region in the 75- to 225-km range has been removed from the array diagram by subtracting each of these four vectors from the anomaly vectors, with the average vector already removed, in the appropriate quadrants of the array diagram. After this has been done, the effect of the region in the 225- to 375-km depth range can be considered and analyzed in a similar manner. The analysis can then be extended to the other regions shown in Fig. III-6 extending to a depth of 975 km. Thus, it might be possible to use this analysis to determine the effect on the array diagram of the crust, upper- and mid-mantle structure under LASA. It should be remarked that this is a first attempt at analysis of the array diagram, and is certainly not the best possible. For instance, the array diagram is expressed in terms of nonorthogonal functions (namely, means valid for the whole segment). Nevertheless, these early results have some interest.

The analysis procedure described previously has been applied to the array diagram at LASA. The original data consisted of 2253 error vectors. However, in order to provide uniform coverage

in the array diagram, a data decimation scheme was used in which the array diagram was divided into a grid of 20 × 20 cells, where each cell is a square of 1 × 1 sec/deg. The first ten vectors to fall within a given cell were taken as acceptable data. This led to a total of 299 error vectors as shown in Fig. III-7. The average of these error vectors was computed and found to point in the direction corresponding to an azimuth of 15°, with a modulus of 0.32 sec/deg, which is in reasonable agreement with the corresponding results of Davies and Sheppard.[5] This mean vector could be associated with a plane-dipping interface which dips down at an azimuth of 15°. These parameters could be associated with a mean dip of 4° of the Moho under LASA, although the Moho is not necessarily the only source of anomaly.

In Fig. III-8, we have the sum of the average vector and all the vectors obtained using the sub-averaging method described previously. The great similarity of the array diagram in Fig. III-8 with that in Fig. III-7 should be noted. This similarity is also borne out by the smallness of the vectors shown in Fig. III-9, which depicts the difference between the error vectors in Figs. III-7 and III-8. The mean-square value of the error vectors shown in Fig. III-9, relative to that in the original array diagram shown in Fig. III-7, is about −10.7 dB. This means that the analysis procedure has been able to remove more than 90 percent of the original error vectors, when measured in terms of mean-square value.

It is also possible to find the mean-square value of the error vectors in each depth range, relative to that in the original array diagram shown in Fig. III-7. The results of such a computation are shown in Fig. III-10, where the ordinate has been labeled as relative amount of heterogeneity. It is seen from this figure that there is an approximately decreasing amount of heterogeneity as the depth increases. This agrees roughly with our notion that the earth becomes more homogeneous as the depth increases. A similar analysis has been performed at NORSAR and the results will be presented.

<div align="right">J. Capon</div>

REFERENCES

1. Seismic Discrimination SATS, Lincoln Laboratory, M.I.T. (31 December 1972), DDC AD-757560.

2. R. E. Needham and D. Davies, "Evidence for Lateral Heterogeneity in the Deep Mantle from Seismic Body Wave Amplitudes," Nature (in press).

3. E. B. Manchee and D. H. Weichert, "Epicentral Uncertainties and Detection Probabilities from the Yellowknife Seismic Array Data," Bull. Seismol. Soc. Am. 58, 1359-1377 (1968).

4. L. P. Vinnik and A. V. Nikolayev, "The Velocity Profile of the Lower Mantle from Direct Measurements of $dT/d\Delta$," Izv. Akad. Nauk. Fiz. Zemlya 11, 24-40 (1970).

5. D. Davies and R. M. Sheppard, "Lateral Heterogeneity in the Earth's Mantle," Nature 239, 318-323 (1972), DDC AD-758942.
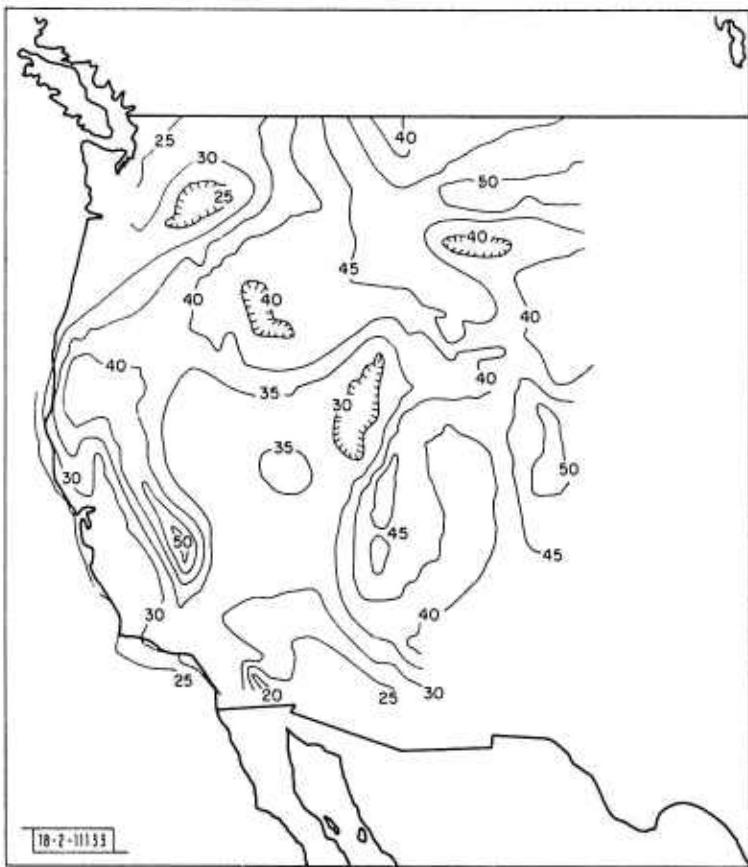
Fig. III-1. Elevation of Mohorovicic discontinuity (km below sea level) in western United States, based on all available data (primarily from seismic refraction measurements). Contour interval is 5 km.
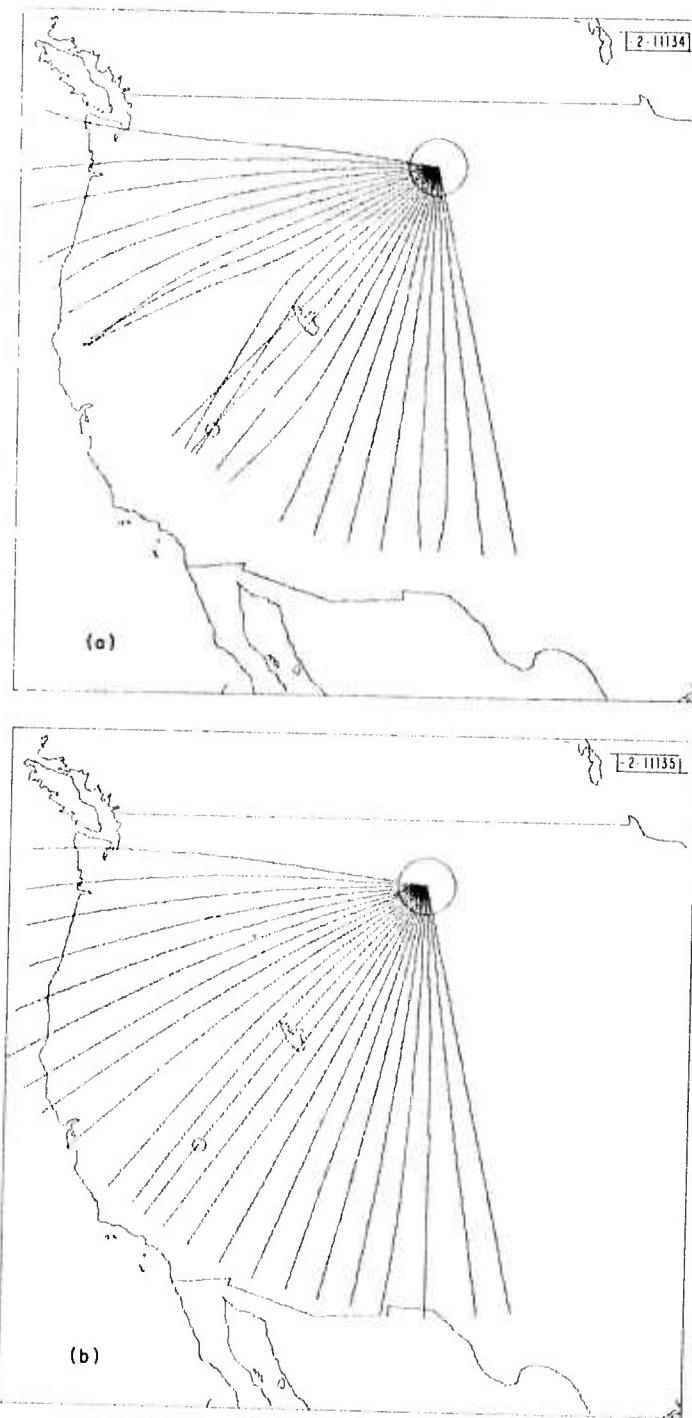
Fig. III-2. Predicted Rayleigh-wave phase ray paths originating at LASA (large circle) for four periods: (a) 10 sec, (b) 20 sec, (c) 30 sec, (d) 40 sec. Azimuth at LASA ranges from 170° to 280° in 5° steps. Nevada Test Site is indicated by small circle.

(c)

(d)
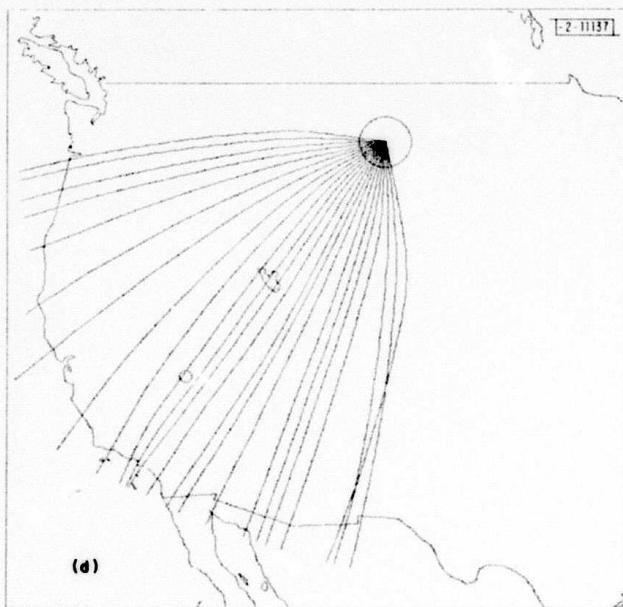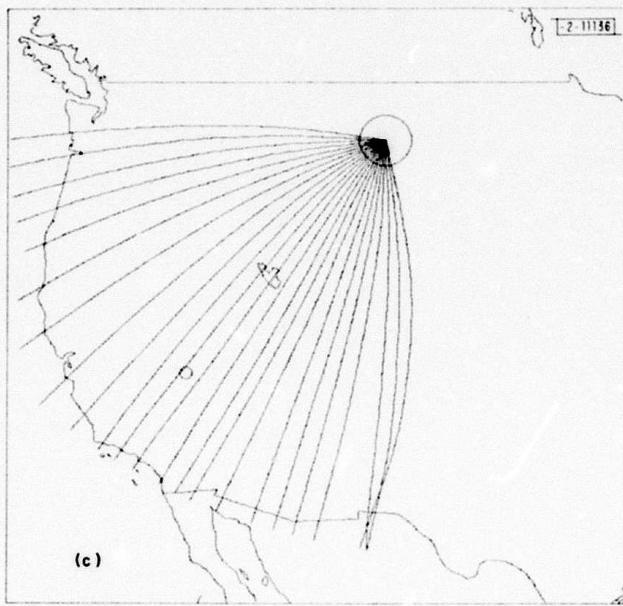
Fig. III-2. Continued.

34
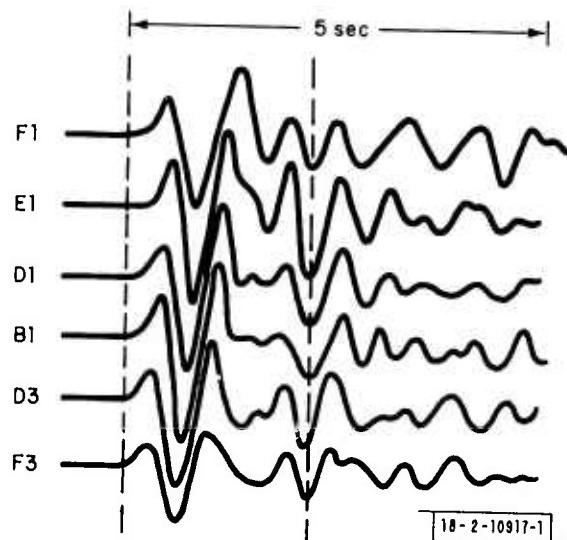
Fig. III-3. Short-period waveforms at LASA for an event in Hindu Kush.
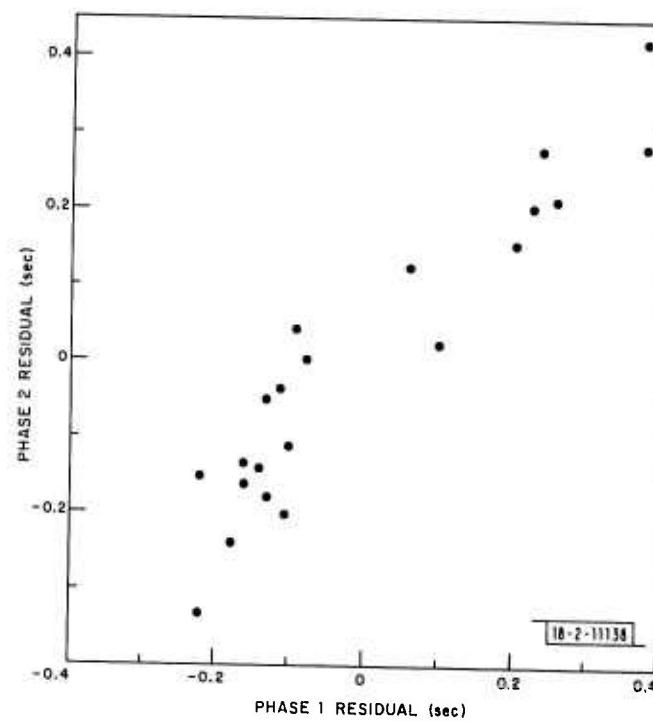
Fig. III-4. Comparison of residuals at LASA subarrays to two plane wave fits. X-axis is residual to first phase; y-axis is residual to second phase. Each point represents one subarray.
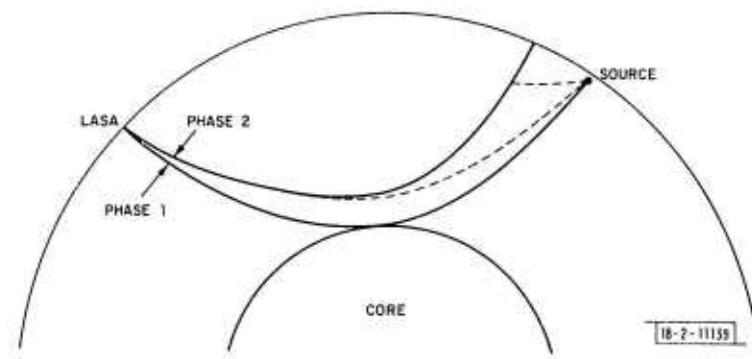
Fig. III-5. Exaggerated sketch of possible ray paths to generate multiple signals at LASA.
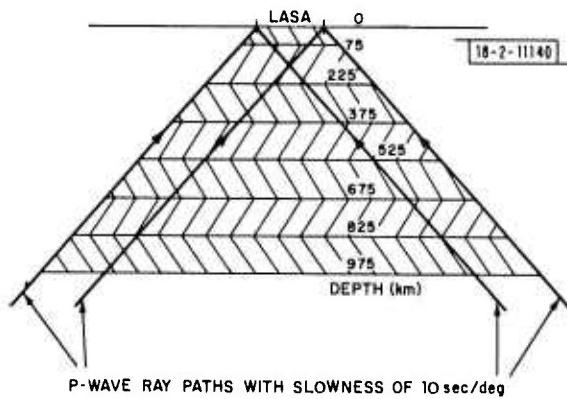
Fig. III-6. Decomposition of region directly under LASA.

10 sec / deg
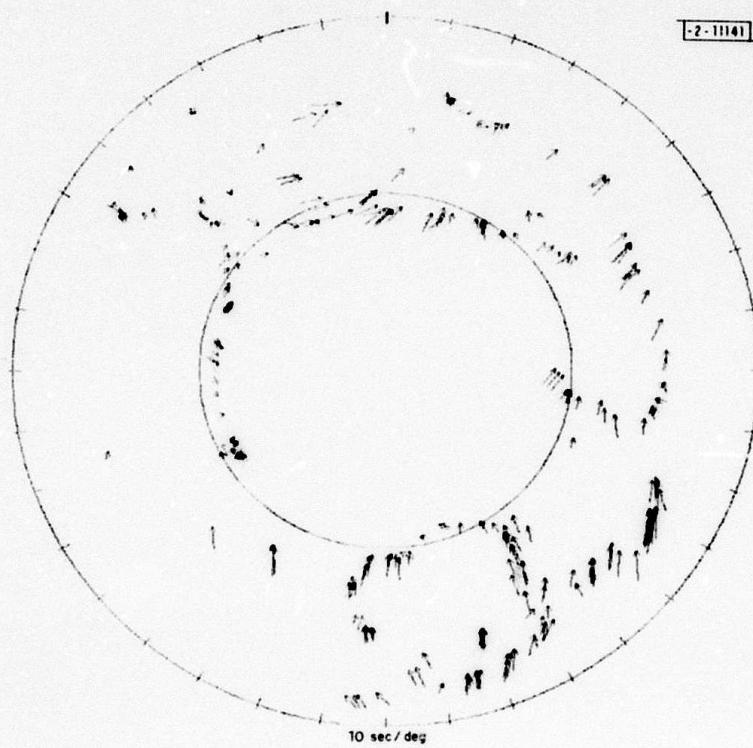
Fig. III-7. Original data used in analysis of array diagram.

2 - 11142

10 sec/deg
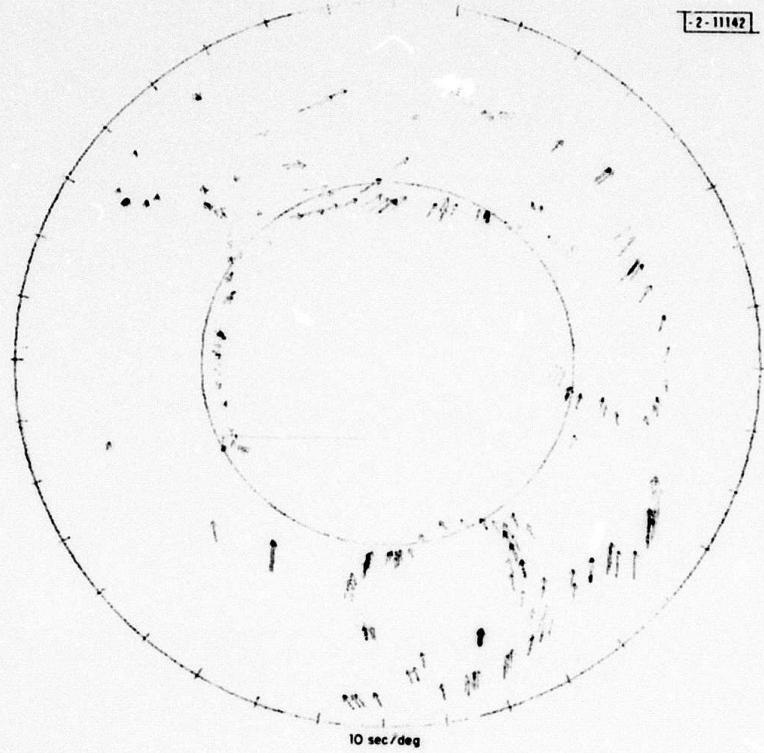
Fig. III-8. Array diagram obtained by adding average and sub-average error vectors.

38

10 sec/deg
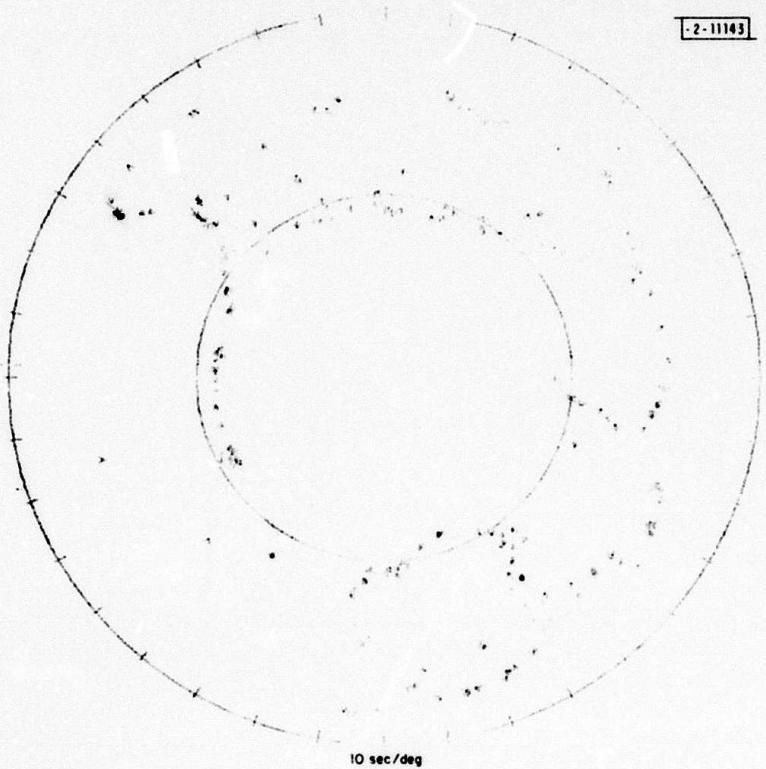
Fig. III-9.   Difference between error vectors shown in Figs. III-7 and III-8.
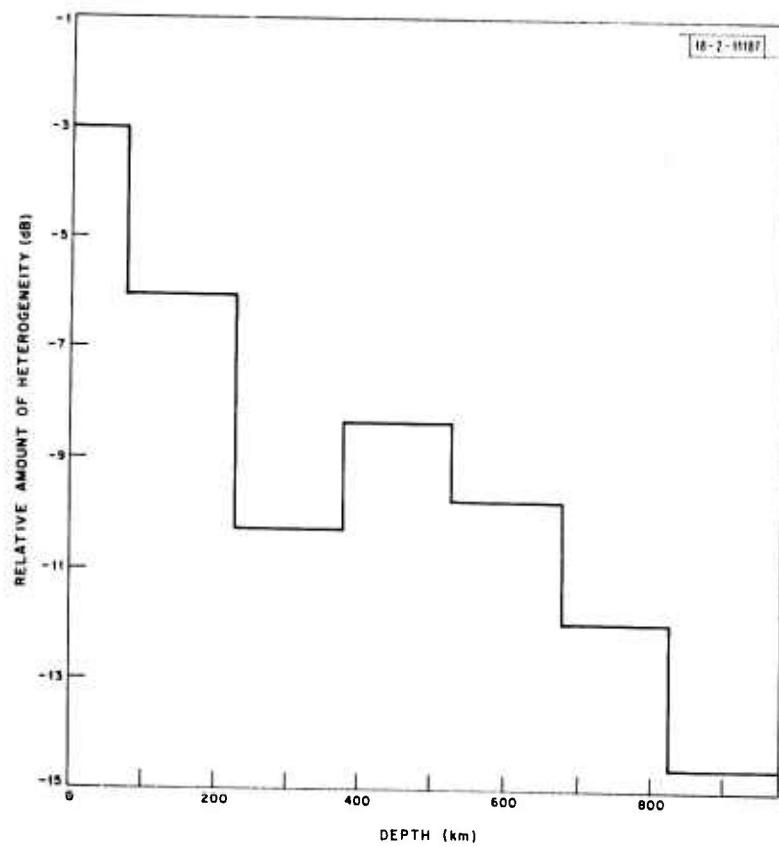
Fig. III-10. Relative amount of heterogeneity vs depth within earth under LASA.

IV. EVASION AND COUNTEREVASION

A. MULTIPLE EXPLOSIONS THAT PRODUCE EARTHQUAKE-LIKE SEISMOGRAMS

Two short-period characteristics of a large class of earthquakes immediately allow them to be discriminated from single explosions. When the rupture time of an earthquake exceeds more than several seconds and when seismic energy is continuously released over that time span, seismograms written at teleseismic distances will be far more complex than those from single explosions even when a large degree of scattering along the explosion-receiver path is present. Further, when the depth phases pP and sP can be identified and when their delay times indicate a hypocentral depth greater than is technically possible to conduct an explosion, then these events are also necessarily earthquakes rather than single explosions. The possibility that these earthquake characteristics could be successfully simulated by spatially and temporally distributing several explosions is investigated.

A constraint on simulating complexity is that the surface- to body-wave energy ratio be consistent with the ratio that would be obtained for an earthquake. Thus, it is necessary to time the explosions so that the short-period body waves do not combine constructively, while the long-period surface waves do. Figure IV-1 shows eight identical source functions with amplitude ratios of 2, 5, 9, 20, 20, 40, 30, 25 and time delays of 0, 1, 2, 4, 6, 7, 8, 9 sec; also shown is the sum of these eight functions. The source function is that of a presumed explosion from Eastern Kazakh of body-wave magnitude 5.5 as recorded at LASA ($\Delta = 83°$). The sum trace is sufficiently complex that such a seismogram could not have been caused by a single explosion. The body-wave magnitude, as conventionally measured in the first several cycles, is smaller than that for the largest single explosion by 0.6. At small epicentral distances, surface waves contain more high-frequency energy and interference should show up more clearly. Consequently, to examine the effect on surface waves, the source Rayleigh wave of an NTS explosion recorded at LASA is used ($\Delta = 12°$). Figure IV-2 shows the result for the Rayleigh wave with the same delays and amplitude ratios. The individual waves sum without significant interference, trebling the maximum amplitude. The result is an increase in surface-wave magnitude of 0.4. Figure IV-3 shows the total effect on the $M_s:m_b$ diagram. The trend lines are those determined by Lacoss.[1] If the $M_s:m_b$ value of the largest single explosion occurred at A, then the decrease in m_b moves the point to B and the increase in M_s moves it to C, which clearly lies within the earthquake population.

It is reasonable to conjecture that the longer the short-period waveform of a given event the greater the source dimensions of that event and consequently, the greater the ratio of long-period energy to short-period energy over small time windows. That is to say, the more complex a body-wave seismogram the higher the M_s. The effect on the $M_s:m_b$ diagram would be that the trend line for complex earthquakes lies to the high M_s side of the overall trend line, and consequently point C may not be in that earthquake population with a comparable complexity. To test this hypothesis, complexity as a function of M_s and m_b is determined. The data set is taken from Lacoss.[1] Figure IV-4 shows the $M_s:m_b$ data and the linear trend, $M_s = 1.6 \, m_b - 4$. $M_s:m_b$ values are projected onto the normal to the linear trend and plotted against Lacoss' complexity values. Thus, complexity on lines parallel to the overall trend line is determined. The result is given in Fig. IV-5; the dashed line is $M_s = 1.6 \, m_b - 4$. The data show two populations. Both groups show increasing complexity as the $M_s:m_b$ trend is traversed toward increasing values of

M_s along the perpendicular to the overall trend. The population with complexity greater than 5 is dominated by shallow earthquakes from the Kurile Islands leading to the conclusion that the magnitude of the phenomenon is a function of source location and/or mechanism. For either population, the result is that the trend line in Fig. IV-3 moves away from point C and so tends to separate the M_s:m_b of the multiple explosion from the earthquake population with comparable complexity. The short-period sum trace has a complexity of 8, and the corresponding position of point C is shown in Fig. IV-5. Thus, the total effect of this series of explosions is not earthquake-like in both M_s:m_b and complexity.

To simulate a pP depth phase requires producing a pulse that is inverted with respect to an earlier arrival. While it is impossible to do it exactly, two characteristics of single-explosion seismograms written on typical short-period instruments make it possible to produce a secondary pulse whose polarity appears inverted. The features are that the basic pulse is essentially monochromatic and that the amplitude of the first half cycle is smaller than several seconds of the early coda. Figure IV-6 shows five of the same source functions with amplitude ratios of 8, 3, 7, 4, 5 and delays of 0, 4, 4.7, 5.1, 7.5 sec and the sum. In the sum, the three apparent arrivals represent P, pP, and sP. The actual first motion of the second arrival is hidden in the coda of the first. Smaller sources are advanced by one cycle and delayed by one-half cycle relative to the second major arrival. The result is an apparent inversion. The quality of the inversion compared to real data is good. The Rayleigh wave, shown in Fig. IV-7, is not significantly enhanced in magnitude and so the M_s:m_b value for the sum is about the same as for either of the two large events. Such a situation does not necessarily enable discrimination, as problem events with similar waveforms exist.[2] The success of the above simulation critically depends on the essentially monochromatic nature of the source waveform. A broadband recording of such a series of explosions would present an entirely different situation.

In conclusion, the possibility of confusing a series of explosions with an earthquake does exist. Whether discrimination can be made by redefining M_s:m_b as a function of complexity, by developing numerical schemes that are capable of detecting closely spaced functions in a seismogram, or by recording broadband, is a subject for future study.

<div align="right">T. E. Landers</div>

B. A STUDY OF LASA EXPLOSION DETECTION CAPABILITY WITHIN THE CODAS OF ASIAN EARTHQUAKES

A simple scheme, employed to estimate the LASA explosion detection capability within the codas of earthquakes from certain Asian regions, consisted of the following steps. The phased sum or beam was formed using the LASA short-period traces of an explosion and an Asian earthquake. In both cases, the beams were aimed at the explosion site. A scaled 20-sec segment of the explosion beam was then repeatedly added to the earthquake coda. A narrow bandpass filter and then a standard detection process were applied to the beam sum. The number of explosions missed by the detection process, as a function of the earthquake-explosion magnitude difference, gave the results of the experiment.

With this study to date, four pairs of explosion-earthquake locations have been considered:

Case I   Explosions – presumed Soviet test site (STS) near Semipalatinsk in Kazakh S.S.R.

                  Earthquakes – Kurile Islands region

Case II   Explosions – STS
               Earthquakes – Kamchatka Peninsula region

Case III   Explosions – hypothetical test site in the Kurile Islands
               Earthquakes – Kurile Islands region

Case IV   Explosions – hypothetical test site near the Kamchatka Peninsula
               Earthquakes – Kamchatka Peninsula

Experiments related to Cases I and II are straightforward since recordings of presumed STS explosions and Kurile Islands and Kamchatka earthquakes exist in our data library. We have no recordings of explosions in the Kamchatka or Kuriles region, but an attempt to synthesize Cases III and IV has been made by adding an STS explosion beam trace, aimed at STS, to a Kurile earthquakes beam when the earthquake beam was formed on a site in the Kurile Islands. An actual Kurile explosion may look quite different than an explosion in central Asia, of course, but the ruse is needed to perform the experiments. The reason that the experiments of Cases III and IV are desirable is that they are, in a sense, extreme cases. We expect earthquake coda attenuation due to beamforming to be a minimum when the array beam is aimed near to the earthquake epicenter.

The detection scheme used here was modeled after that used by the Seismic Array Analysis Center (SAAC) and is described in Ref. 3. The method compares the ratio of a short-term average (STA) rectified signal to a similar long-term average (LTA) and declares a detection when this ratio exceeds a threshold for a certain number of comparisons. No search was made to find an optimum coda detection process; a standard process was used with threshold parameters which gave relatively few false alarms.

The STA was computed using the following formula from Ref. 1:

$$STA(n\Delta t) = P^{-1} \sum_{p=0}^{P-1} |B[(n-p)\Delta t]| \quad .$$

Here, $B(n\Delta t)$ represents the filtered beam sampled at $n\Delta t$. In practice, Δt was set at 0.2 sec and $P = 3$; the STA was computed every 0.6 sec. The LTA was computed using the recursive relation

$$LTA_n = 2^{-\eta} STA_n + (1 - 2^\sigma) LTA_{n-1} \quad .$$

Values of 1 and 4 are used for η and σ, respectively. Because the effective length of this LTA was greater than the 20-sec interval at which explosions were added, the LTA was computed using the filtered earthquake beam to which no explosions had been added. This means that the previously added explosions did not contaminate the LTA upon which the detections were based. The STA of this beam was also computed in order to check for false alarms. If the STA/LTA ratio exceeded 10 dB for three consecutive computations, i.e., 1.8 sec, a detection was declared. An example of the method, as applied to Case III, is given in Fig. IV-8.

The presumed explosion used in this study occurred on 5 September 1968 and was assigned a body-wave magnitude of 5.5 by the U.S. Coast and Geodetic Survey (USCGS). This event was scaled to ten other magnitudes, down to 3.4, in order to represent a wide range in explosion

size. The locations of the explosions, taken for beamforming purposes, and the regions from which the earthquakes were taken are summarized below:

Case	Explosions	Earthquakes
I	50°N, 60°E	40-50°N, 145-155°E
II	50°N, 80°E	50-60°N, 155-170°E
III	45°N, 150°E	40-50°N, 145-155°E
IV	55°N, 160°E	50-60°N, 155-170°E

The detection criterion was applied to the earthquake trace (in order to check for false alarms) and to the 11 earthquake-plus-explosion traces for each of the four cases using 16 earthquakes from the Kurile Islands region and 18 earthquakes from the Kamchatka region. The number of explosions missed (N) was counted in each experiment. If N was less than the number of explosions added before the earthquake, due to high noise conditions, that trace was disregarded. Otherwise, the number of explosions missed was recorded and plotted against the magnitude difference between the earthquake and scaled explosion. These results are given in Figs. IV-9 through IV-12.

Figure IV-9 shows the number of explosions missed, in the conditions of Case I, plotted against the earthquake-explosion difference, $m_q - m_x$. Figures IV-10 through IV-12 give analogous displays for Cases II through IV, respectively. The straight lines drawn on these figures represent the author's estimate of the maximum number of explosions missed as a function of magnitude difference. Although parameterized versions of these lines will be used in the following section to extend these results, the nature of these lines and the distribution of points merit some discussion at this time. Cases I and II (Figs. IV-9 and -10) are similar in that the explosions are from the same site and the earthquakes are from regions contiguous to each other. In spite of this, the scatter of points is greater in Figs. IV-10 and -12 than in Figs. IV-9 and -11; this probably reflects the wider geographic distribution of the earthquakes used in Cases II and IV. It is also of interest to compare the trend of the points in Cases I and II with that of Cases III and IV. The former, although they have a lower zero intercept, exhibit a steeper slope than the latter. The slope of the "maximum number missed" lines is largely controlled by the number of missed detections at high magnitude differences. This leads to the conclusion that the coda from large events becomes increasingly incoherent with increasing time after the first arrival. Alternatively stated, the effectiveness of beamforming on location A to suppress the coda of an event from location B decreases with time after the arrival of the initial P-wave from location B.

The application of the detection scheme to the earthquake trace alone gave rise to nine false alarms in the total of 68 beams processed (two beams for each event in each region). Of these spurious detections, five were due to the surface reflection phase pP, two were due to a small interfering event, and the remaining two were genuine false alarms.

An attempt to extend these results in order to estimate the maximum total time that an explosion of given magnitude in the Kurile Islands, near the Kamchatka Peninsula, or at STS would have gone undetected at LASA due to the long-term seismicity of the Kuriles or Kamchatka region is given in the next section.

<div align="right">J. R. Filson</div>

C. ON ESTIMATING THE EXPLOSION MASK TIME AT LASA DUE TO THE SEISMICITY OF CERTAIN REGIONS

In this section, an attempt is made to extend the results of Sec. B in an effort to estimate the detection capability of LASA over an extended period of time for each of the four cases

previously discussed.   Let the functions M, E, and τ be defined as follows:

$M(m_q, T, s_2)$ — The number of earthquakes of magnitude m_q that occurred in the region s_2 over the extended period of time T

$E(m_q - m_x, s_1, s_2)$ — An estimate of the time that an explosion of magnitude m_x at site s_1 would go undetected at LASA in the P-wave coda of an earthquake of magnitude m_q from region s_2

$\tau(m_x, T, s_1, s_2)$ — An estimate of the total time that an explosion of magnitude m_x at site s_1 would have gone undetected due to the natural seismicity of region s_2 over the time period T.

The assertion is made that the total mask time τ may be represented as

$$\tau(m_x, T, s_1, s_2) = \sum M(m_q, T, s_2)\, E(m_q - m_x, s_1, s_2) \tag{IV-1}$$

where the summation is over m_q.

The results of Sec. B give us an opportunity to estimate E and thus τ using published seismicity lists.   The straight lines on Figs. IV-9 through IV-12 represent the maximum number of explosions (N), spaced at 20-sec intervals, that would be missed at LASA for an earthquake-explosion magnitude difference $m_q - m_x$.   These lines are of the form

$$N(m_q - m_x, s_1, s_2) = \delta \exp[\xi (m_q - m_x)] \tag{IV-2}$$

where the parameters δ and ξ depend on s_1 and s_2.   The values of these parameters for each of the four cases are given below:

Case	s_1	s_2	δ	ξ
I	STS	Kuriles	1.9	1.66
II	STS	Kamchatka	2.9	1.64
III	Kuriles	Kuriles	4.5	1.20
IV	Kamchatka	Kamchatka	5.5	1.26

Once N has been evaluated for a given case and a given $m_q - m_x$, it may be used to estimate E by

$$E(m_q - m_x, s_1, s_2) = \Delta t \cdot N(m_q - m_x, s_1, s_2) \quad . \tag{IV-3}$$

Here, Δt is the time interval at which the explosions were added (20 sec) and E now is an estimate of the maximum mask time due to an event magnitude difference $m_q - m_x$.   Equations (IV-2) and (IV-3) make possible the use of Eq. (IV-1) in order to estimate τ.

There are certain qualifications that must be made before the results of such estimates are discussed. The time period T was taken as the decade 1963 to 1972, and the USCGS and NOS seismicity lists for this period were used to determine the function M. Although these lists may lack sensitivity below a certain magnitude, they represent the most stable source of world-wide seismicity information over an extended period of time. Figures IV-13 and -14 show the cumulative seismicity distribution for the Kurile Islands and the Kamchatka Peninsula for the period 1963 to 1972. The Kurile Islands region was taken as 40-50°N and 145-155°E, the Kamchatka region 50-60°N and 155-170°E. These curves exhibit the familiar flattening feature at low magnitudes due to the insensitivity of the location network. This insensitivity is probably significant below $m_b = 4.5$ in both regions.

This effect gives rise to a specific qualification on the use of Eqs. (IV-1) through (IV-2) and (IV-3). Because of the form given Eq. (IV-1), the values assigned to its parameters, and the detection scheme used, an explosion may be hidden by an earthquake of a smaller magnitude. Thus, in order to estimate the total time that a magnitude 4.5 explosion would be hidden, the total number of magnitude 4.3 earthquakes is required. Since the seismicity function M is certainly incomplete at magnitude 4.3, an estimate of τ for $m_x = 4.5$ must certainly be low. The severity of this effect increases with the value of the parameter δ. In the use of Eq. (IV-2), all fractional detections were rounded down to the nearest integer before using N in Eq. (IV-3). This is a fairly safe procedure because all of the points of Figs. IV-9 through IV-12 lie below the straight lines. It is also a necessary procedure since large negative values of $m_q - m_x$, even though they might give rise to values of $0 < E \ll 1$ if N was allowed to float, appreciably contribute to τ for M large and m_q small. In this case, the explosion would be the much larger arrival on the record and there would be no question of a much smaller earthquake hiding it. In the light of the above discussion, the condition that

$$\delta \exp[\xi(m_q' - m_x)] < 1.0 \qquad\qquad (IV-4)$$

when estimating τ for a given m_x, where m_q' is the magnitude above which $M(m_q, T, s_2)$ is believed to be complete, assures the validity of τ in the context of the experiment.

Figures IV-15 through IV-18 show the results of the method for Cases I through IV, respectively. The estimates of τ in these figures are maximum estimates in the sense that the parameters of Eq. (IV-2) were chosen for a line that lay above all the data points. Thus, the ordinate in these figures represents the maximum estimate of total time in minutes during the 10-year period that an explosion of magnitude m_x, at the site indicated, would have gone undetected due to the seismicity of either the Kurile Islands or the Kamchatka region. The arrows on these figures indicate an m_x below which the estimates are not strictly valid. The placing of these arrows is based on the condition of Eq. (IV-4) where $m_q' = 4.5$. This implies that the seismicity data are considered complete down to $m_q = 4.5$. If the reader chooses to pick an alternate m_q', these arrows will be shifted to the right or left of the number of magnitude units that the new m_q' differs from 4.5. The straight solid lines on these figures represent an approximation of the linear extension of the points to the right of the arrows, to m_x values to the left of the arrows where the plotted points are considered to be low.

As an example, these figures allow us to estimate the maximum total time that an explosion of magnitude 5.5 would have gone undetected at LASA during the 10-year period (1963 to 1972) for each of the four cases. The results are summarized below:

Case	Total Mask Time
I	205 minutes (3.4 hours)
II	135 minutes (2.3 hours)
III	Approximately 2000 minutes (33.4 hours)
IV	Approximately 1000 minutes (16.7 hours)

Again, these estimates are, in a sense, maximum ones and they refer to only one array at which a standard detection scheme, not specialized for coda detection, was applied.

J. R. Filson

REFERENCES

1. R. T. Lacoss, "A Large-Population LASA Discrimination Experiment," Technical Note 1969-24, Lincoln Laboratory, M.I.T. (8 April 1969), DDC AD-687478.

2. T. E. Landers, "Some Interesting Central Asian Events on the $M_s:m_b$ Diagram," Geophys. J. R. Astr. Soc. 31, 329-339 (1972).

3. "Seismic Array Design Handbook," Federal Systems Division, International Business Machines (August 1972).
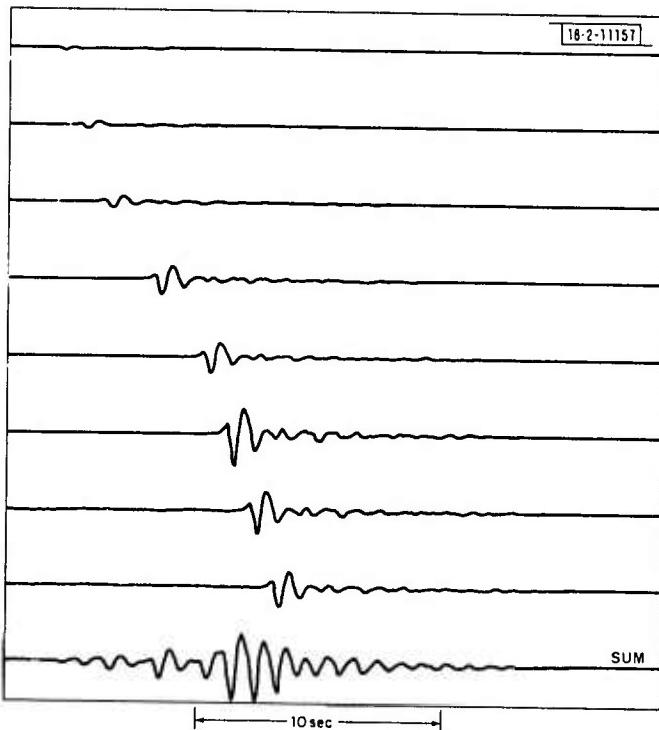
Fig. IV-1. Sum of eight identical short-period waveforms to simulate a complex seismogram.
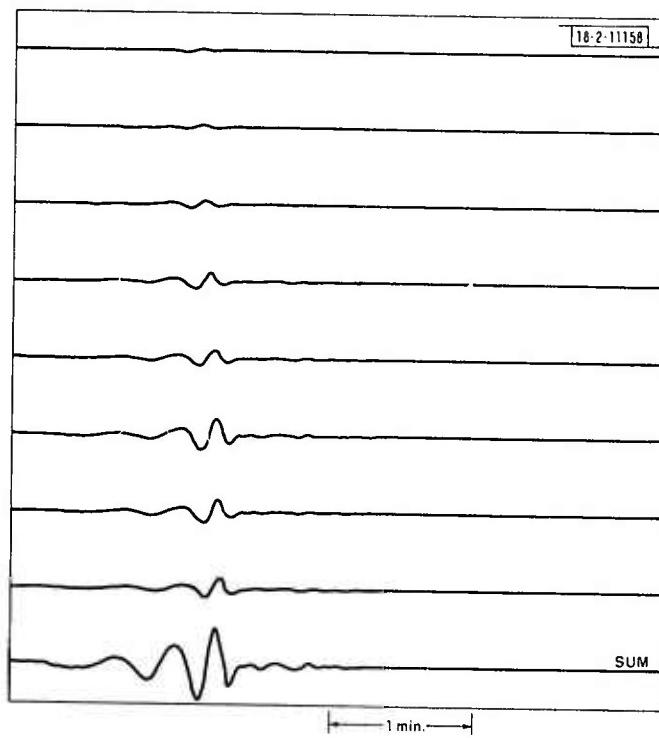
Fig. IV-2. Same as Fig. IV-1 for Rayleigh wave.
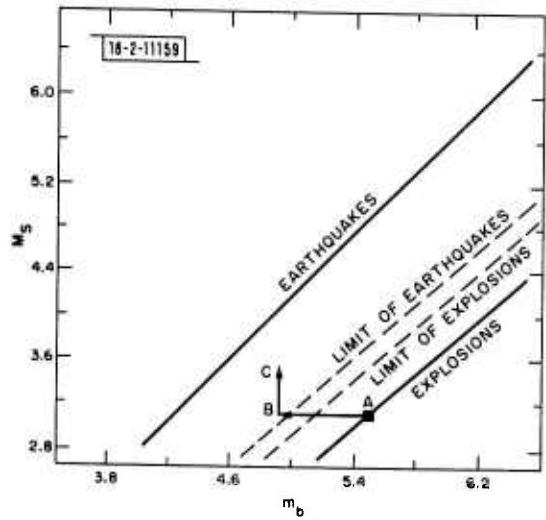
Fig. IV-3. If $M_S{:}m_b$ value of largest single event in Fig. IV-1 is at A in explosion population, value for sum is at C in earthquake population.
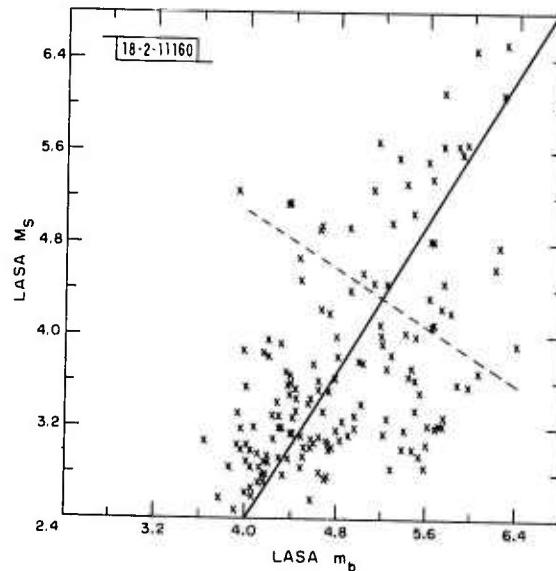
Fig. IV-4. $M_S{:}m_b$ data base used in determining how complexity varies across population (dashed line).
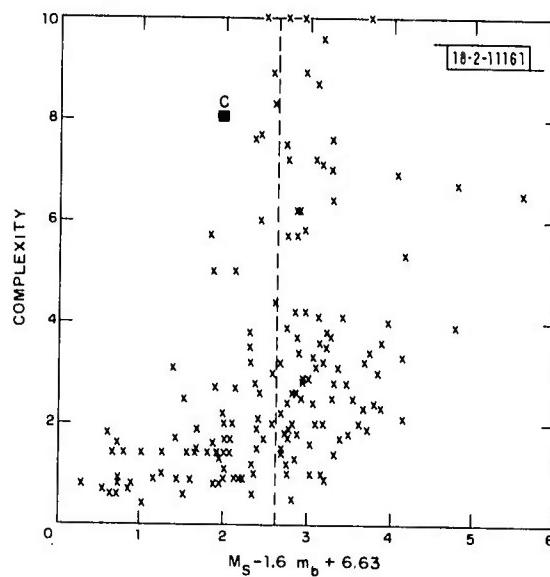
Fig. IV-5. Complexity on lines parallel to linear trend (solid line in Fig. IV-4). Dashed line is $M_S = 1.6\,m_b - 4$.
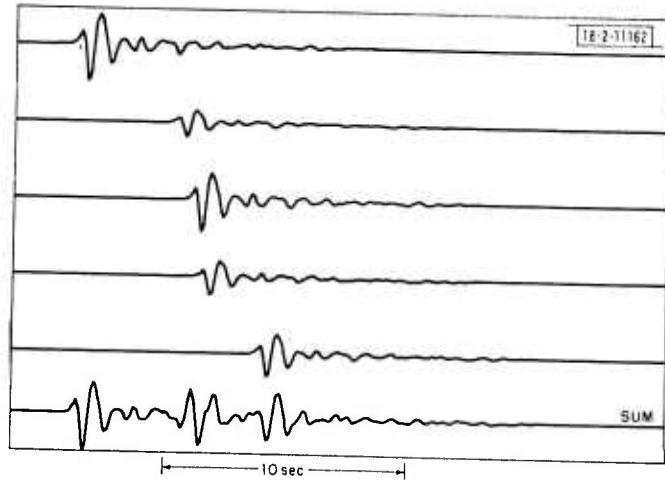
Fig. IV-6. Sum of eight identical short-period waveforms to simulate pP.
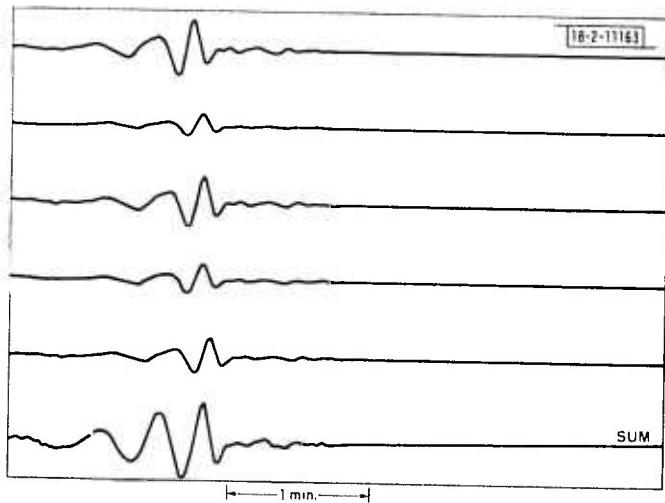
Fig. IV-7. Same as Fig. IV-6 for Rayleigh wave.
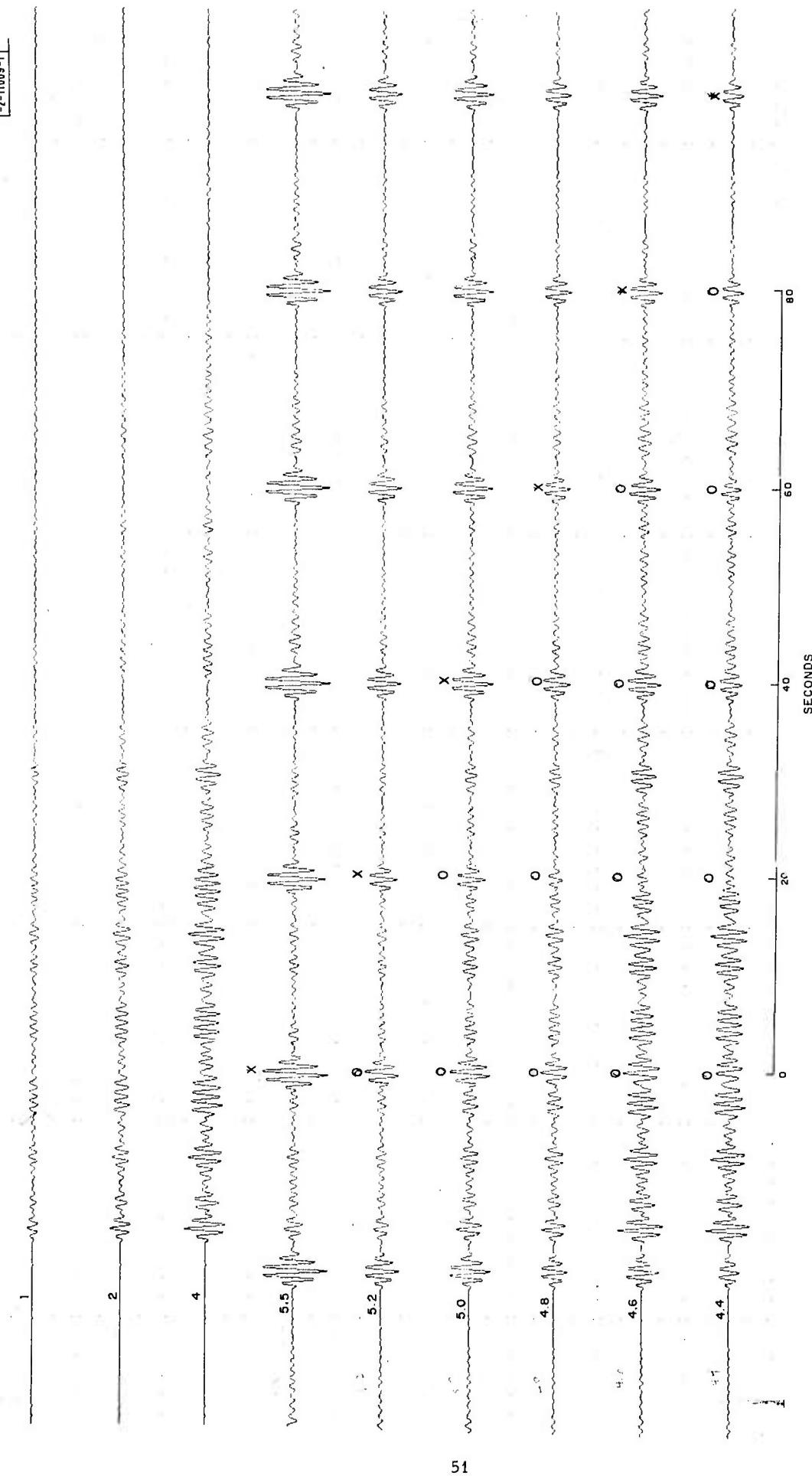
Fig. IV-8. Example of result of adding explosion traces to an earthquake coda. Top three traces represent filtered beam of earthquake (m_b = 4.6) in Kurile Islands aimed at hypothetical explosion site in Kurile Islands; it is shown at three gain levels: 1, 2, and 4. Lower six traces show explosions of magnitude 5.5 and 5.2 added to earthquake and shown at gain 1; explosions of magnitude 5.0 and 4.8 added to earthquake, gain 2; and explosions of magnitude 4.6 and 4.4 added to earthquake, gain 4. First explosion detected following earthquake is marked X; undetected explosions are marked O.

51
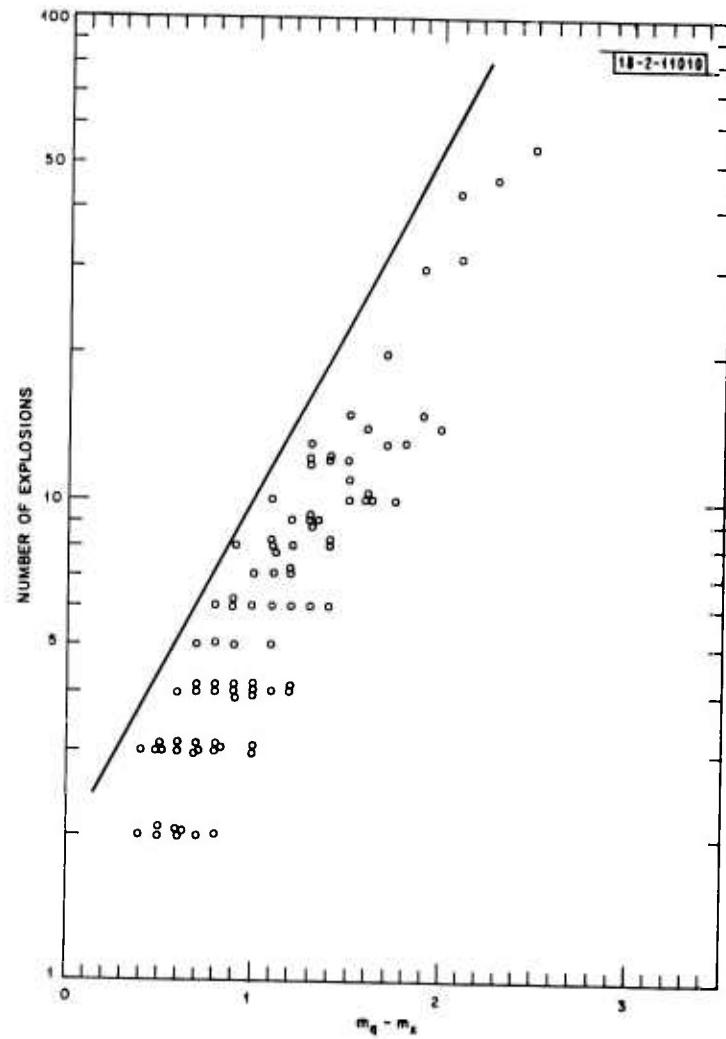
Fig. IV-9. Points represent number of STS explosions undetected on LASA beam aimed at STS, due to Kurile Islands earthquakes. These points are plotted vs magnitude difference ($m_q - m_x$) between earthquake (m_q) and explosion (m_x). This figure is relevant to Case I described in text. Straight line represents author's estimate of maximum number of explosions missed as a function of magnitude difference. Explosions were added at 20-sec intervals.
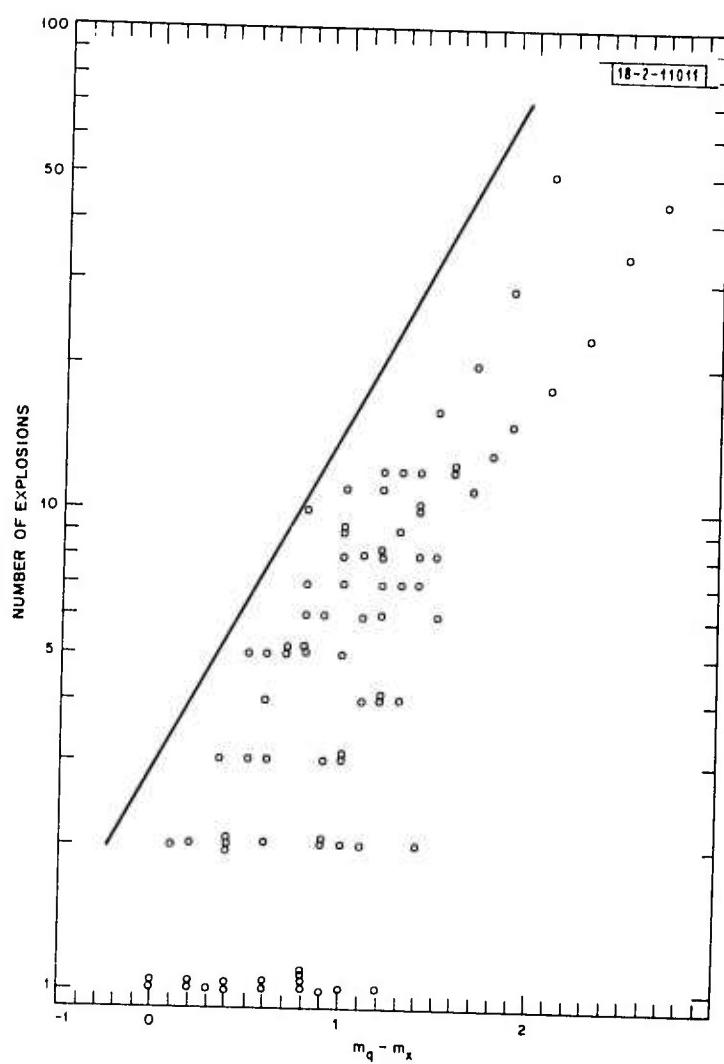
Fig. IV-10. Diagram analogous to Fig. IV-9 and relevant to Case II. STS explosions undetected on LASA beam aimed at STS due to Kamchatka earthquakes.
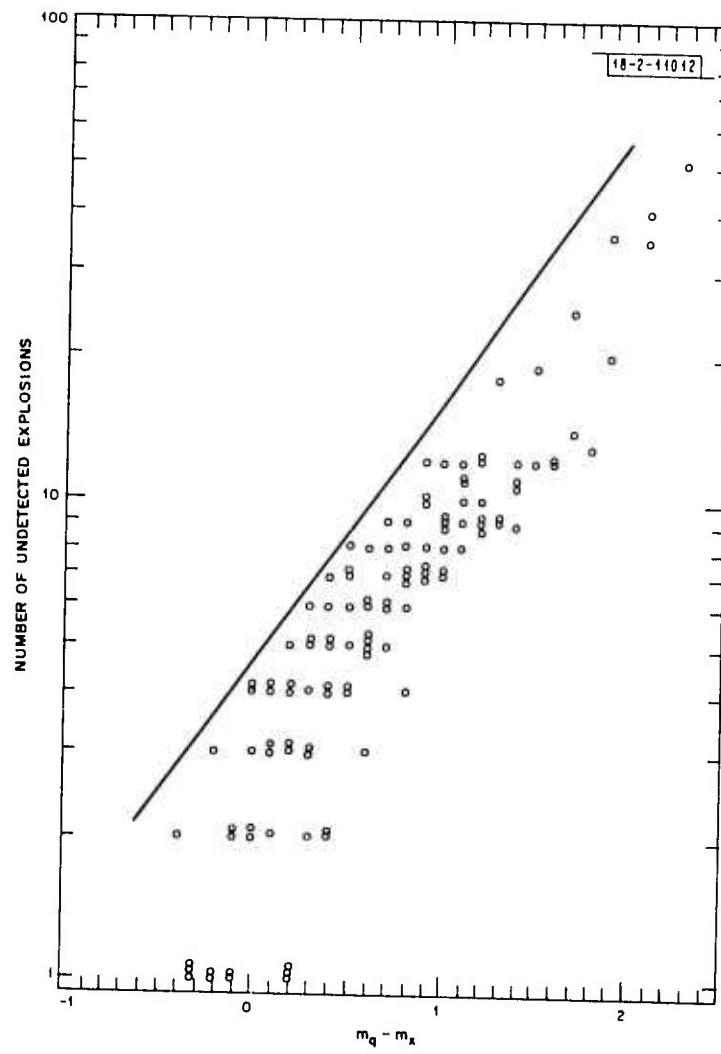
Fig. IV-11.   Diagram analogous to Fig. IV-9 and relevant to Case III.   Hypothetical Kuriles explosions undetected on LASA beam aimed at Kurile Islands due to Kurile Islands earthquakes.
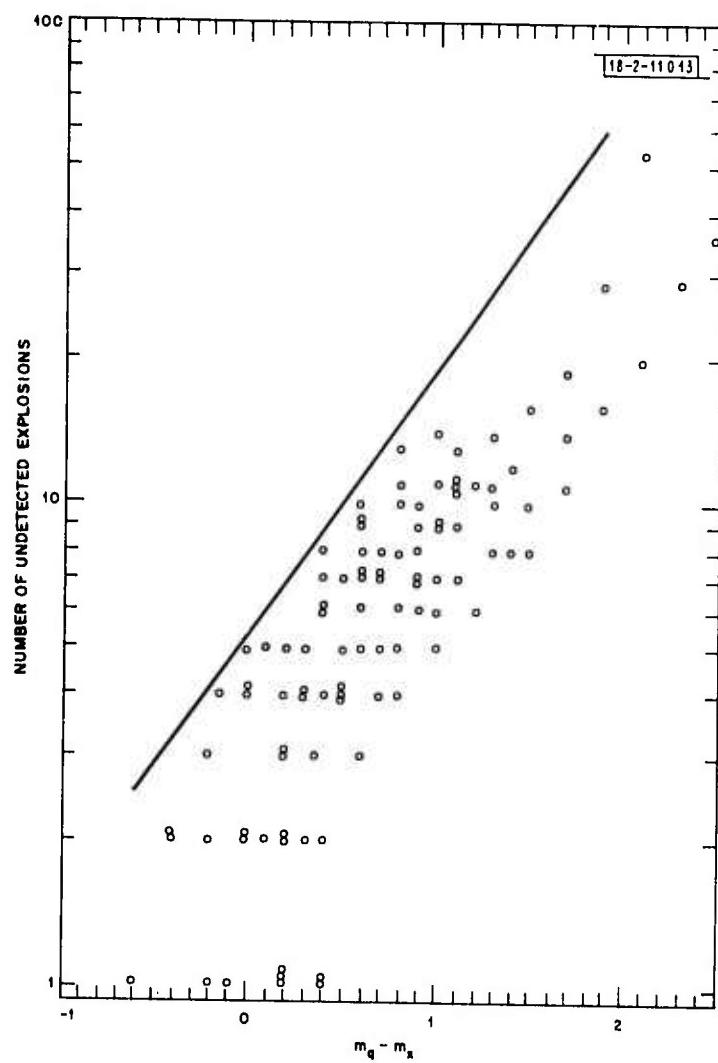
Fig. IV-12.   Diagram analogous to Fig. IV-9 and relevant to Case IV.
Hypothetical Kamchatka explosions undetected on LASA beam aimed
at Kamchatka due to Kamchatka earthquakes.
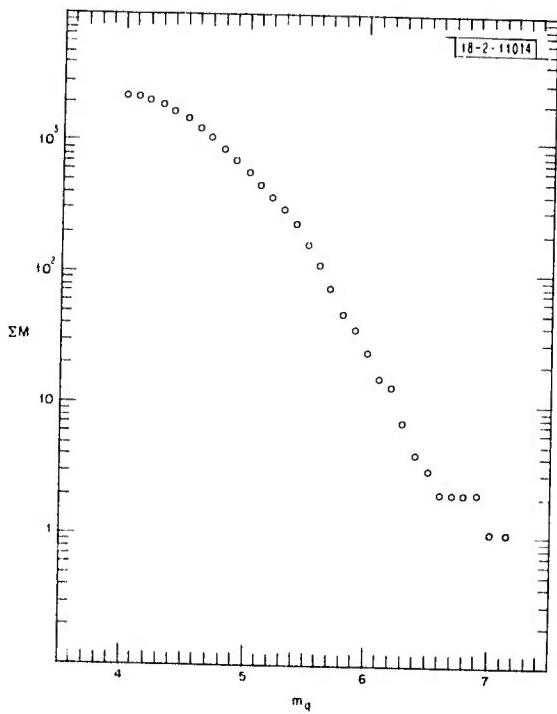
Fig. IV-13. Points represent total number of earthquakes of given magnitude (mq) or greater reported by USCGS during 1963 to 1972 as occurring in Kurile Islands region 40-50°N, 145-155°E.
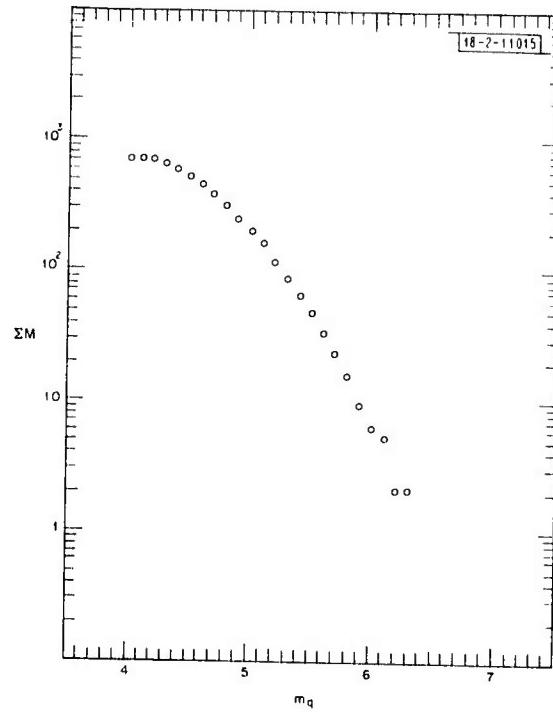
Fig. IV-14. Points represent total number of earthquakes of given magnitude (mq) or greater reported by USCGS during 1963 to 1972 as occurring in Kamchatka region 50-60°N, 155-170°E.

Fig. IV-15.   Result of applying Eq. (IV-1) to data of Figs. IV-9 and -10, Case I. Points represent estimate of maximum time (in minutes) that magnitude m_x explosion at STS would have gone undetected by LASA due to Kurile Islands seismicity during decade 1963 to 1972.   Arrow represents magnitude below which results are not considered strictly valid.   Line represents approximate linear extension of points at magnitudes greater than that of arrow.
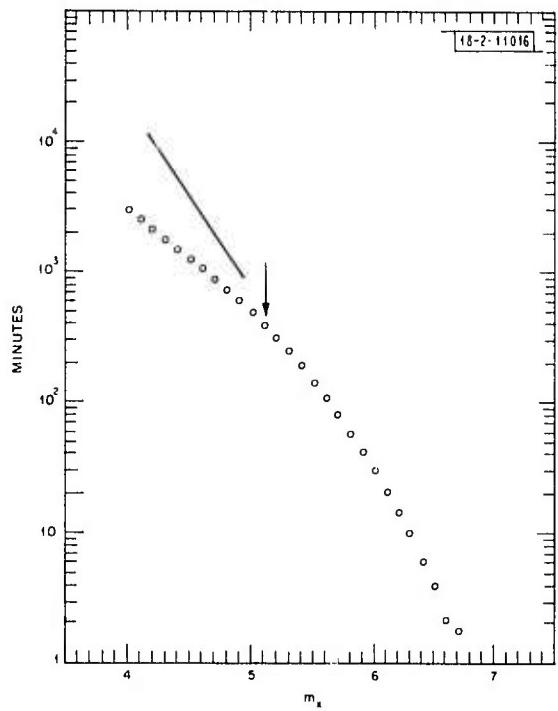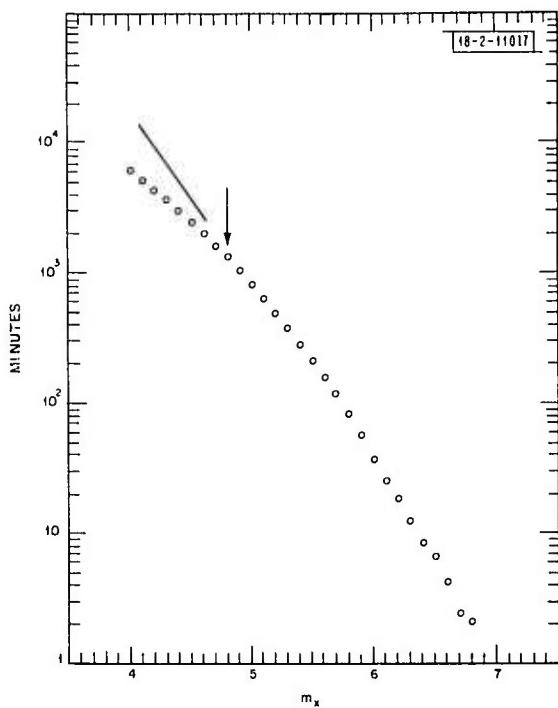
Fig. IV-16.   Diagram analogous to Fig. IV-15 and relevant to Case II.   Points represent estimate of time (in minutes) that magnitude m_x explosion would have gone undetected by LASA due to Kamchatka seismicity during decade 1963 to 1972.
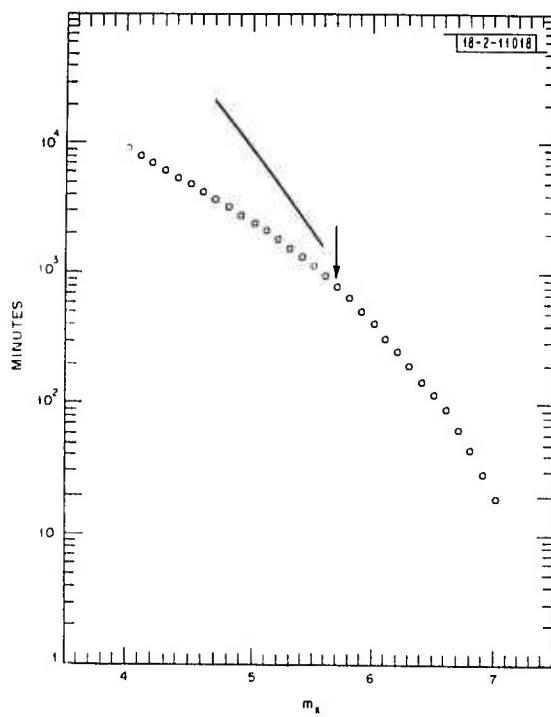
Fig. IV-17. Diagram analogous to Fig. IV-15 and relevant to Case III. Points represent estimate of time (in minutes) that hypothetical, magnitude m_x explosion in Kurile Islands would have gone undetected by LASA due to Kurile Islands seismicity during decade 1963 to 1972.
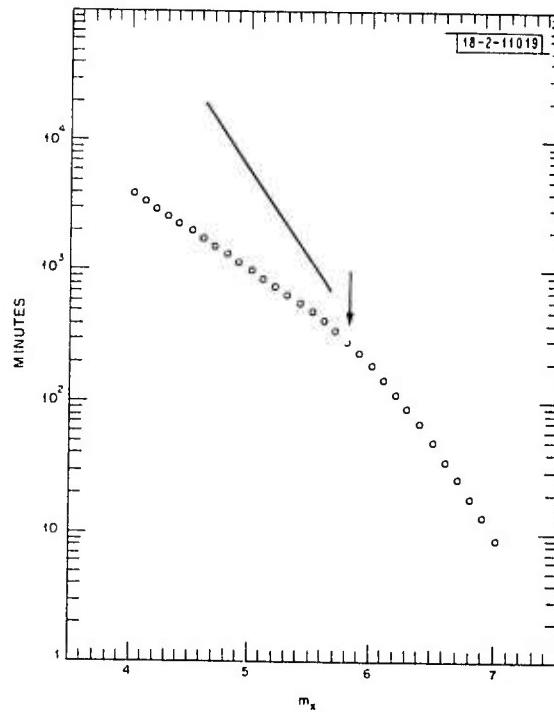
Fig. IV-18. Diagram analogous to Fig. IV-15 and relevant to Case IV. Points represent estimate of time (in minutes) that hypothetical explosion of magnitude m_x near Kamchatka Peninsula would have gone undetected by LASA due to Kamchatka seismicity during decade 1963 to 1972.

V. GENERAL SEISMOLOGY

OBSERVATIONS OF PcP AND P PHASES AT LASA AT DISTANCES FROM 40° to 84°

In the SATS dated 31 December 1972 (DDC AD-757360), we reported observations of P and PcP amplitudes in the distance range 26° to 40° from LASA. Here, we extend the range of observation with data from 40° to 84° distance with depths from 0 to 600 km. Included in the population are the explosion LONGSHOT, and four presumed Soviet explosions — one in the Ural mountains, two from Novaya Zemlya, and one from Eastern Kazakh.

In studies of the core-mantle boundary, one of the perplexing features of short-period data has been that observed PcP/P ratios are strongly scattered, with average values several times larger than predicted by reasonable earth models. There are many possible causes for this phenomenon, summarized by Vinnik and Dashkov,[1] but one popular explanation is that the earth has low Q values for P-waves. Kanamori[2] found that some of the scatter for events of different depth could be reduced by assuming a highly attenuative earth with Q values for short-period compressional waves which are comparable to Q values for longer-period shear waves. Ibrahim[3] studied P and PcP data from explosions only, and deduced that a Q model similar to Kanamori's would be required to reduce the data scatter.

This has created somewhat of a paradox because short-period attenuation studies by Asada and Takano,[4] Archambeau et al.,[5] Frasier and Filson,[6] and others show that Q values for short-period P-waves are an order-of-magnitude higher than those deduced by Kanamori.

We present LASA data here showing that PcP/P ratios are a strong function of focus depth. However, we also demonstrate that low Q models do not adequately resolve the problem and that the scatter in PcP/P ratios is due to amplitude fluctuations of P rather than PcP waves.

Figure V-1 shows the distribution of data in depth and distance from LASA. The open circles are events to the southeast of LASA within an azimuthal sector from 131° to 151°. The solid circles are events to the northwest within the sector 303° to 319°. Also shown by x's are the explosion LONGSHOT and four presumed Soviet explosions. The Soviet events all have azimuths nearly due north from LASA.

The steered beams for about half the data used in this study are displayed in Fig. V-2. Each pair of traces consists of a P beam above the corresponding PcP beam, for the same event, normalized for display purposes to approximately the same gain. The events are arranged vertically in order of increasing distance. Those events marked S are from the southeast sector from LASA, all others being from the northwest. By steering beams for each phase, the receiver crustal variations from sensor to sensor are minimized and the noise is reduced.

In Fig. V-3, the PcP/P ratios of A/T for the LASA beams are shown vs epicentral distance. The curve is the theoretical PcP/P ratio predicted by Johnson's CIT 208 earth velocity model,[7] assuming the B1 core-mantle model of Bullen and Haddon.[8] No earth attenuation has been included in the model. Because of this, the theoretical curve varies insignificantly with depth of focus, and may be taken to represent all depths.

A noticeable feature of the data is the discontinuity around 60°, where most of the PcP/P data suddenly drop from above to below the curve. This is clearly a depth effect. Almost all the data above the curve for delta less than 60° have shallow depths less than 200 km. Data below the curve with delta greater than 60° are almost all deep events. The five explosions are all above the curve. The earthquake at 68°, nearly coincident with the explosion, has an NOS depth

fixed at 33 km. At 58°, the solid circle below the curve has a depth of 393 km, and has a PcP/P ratio several times lower than the shallow events at the same delta.

This effect is more clearly seen in Fig. V-4 where the PcP/P data are plotted vs depth of event. Here we see that the explosion data at zero depth are grouped with shallow earthquakes, with PcP/P ratios 3 to 4 times those for the deep events. Figure V-5 shows the data of Fig. V-4 after normalizing all ratios to a distance of 60°. This was done by removing the trend of the theoretical curve in Fig. V-3 from the data of Fig. V-4. Thus, PcP/P ratios at distances greater than 60° were amplified to remove the effect of spherical spreading and core reflection. One sees that the scatter of PcP/P ratios in Fig. V-5 is less than in Fig. V-4, and that this depth dependence is clearly in the data.

If we now correct the observed PcP/P data for Kanamori's Q model, that is, remove the attenuation effects, we obtain the data shown vs distance in Fig. V-6. We see that the PcP/P ratios have been lowered everywhere so that they are almost all below the theoretical curve. However, the scatter of data has not been significantly reduced. The PcP/P ratios at 40° have been severely attenuated and the explosions are still significantly above the deep event populations. These PcP/P ratios are normalized to a delta of 60° and plotted vs depth in Fig. V-7; this figure shows that the depth effect persists in spite of the strong attenuation corrections which have been made. This indicates that the scatter of PcP/P ratios cannot be caused by a laterally homogeneous, low Q model of the earth.

In Fig. V-8, the PcP amplitudes are shown with each event normalized to LASA $m_b = 6.0$, using the Gutenberg-Richter magnitude formula.[9] The curve shows the theoretical PcP amplitude for the unattenuated earth model. It is adjusted in amplitude to pass through the data. The PcP amplitudes show no separation between deep and shallow events. In fact, the trend of data from 50° to 83° is well-defined with less scatter than seen in the PcP/P ratios.

This suggests that the Gutenberg-Richter B factor, which strongly depends on focal depth for all distances, applies to P data but not to PcP amplitudes. That is, magnitude-6 events located at various depths produce a relatively smooth PcP curve without any further depth corrections.

Figure V-9 shows the PcP amplitudes of Fig. V-8 plotted as a function of depth and normalized to $\Delta = 60°$ by removing the trend of the curve in Fig. V-8. We see that the clear depth trend of the data has disappeared, and the explosion data at zero depth are more consistent with the deep focus data.

The conclusion to be drawn from these data is that the scatter of PcP/P ratios at LASA is primarily caused by the depth effect on P-waves, which is given by the empirical B factor of Gutenberg and Richter.[9] This B factor cannot be produced by attenuation and spreading of rays in laterally homogeneous earth models. Other scattering mechanisms are being investigated to explain this phenomenon.

<div style="text-align: right">

C. W. Frasier
D. K. Chowdhury*

</div>

* Indiana University.

REFERENCES

1. L. P. Vinnik and G. G. Dashkov, "Reflections from the Core Caused by Atomic Explosions and Problems of the Earth's Internal Structure," Dokl. Acad. Nauk. SSSR. 184, 10-13 (1969).

2. H. Kanamori, "Spectrum of P and PcP in Relation to the Mantle-Core Boundary and Attenuation in the Mantle," J. Geophys. Res. 72, 559-571 (1967).

3. A. B. Ibrahim, "The Amplitude Ratio PcP/P and the Core-Mantle Boundary," Pure Applied Geoph. 91, 114-133 (1971).

4. T. Asada and K. Takano, "Attenuation of Short Period P Waves in the Mantle," J. Physics of the Earth 11, 25-34 (1963).

5. C. B. Archambeau, E. A. Flinn and D. G. Lambert, "Fine Structure of the Upper Mantle," J. Geophys. Res. 74, 5825-5865 (1969).

6. C. W. Frasier and J. Filson, "A Direct Measurement of the Earth's Short Period Attenuation Along a Teleseismic Ray Path," J. Geophys. Res. 77, 3782-3787 (1972).

7. L. R. Johnson, "Array Measurements of P Velocities in the Lower Mantle," Bull. Seismol. Soc. Am. 59, 973-1008 (1969).

8. K. E. Bullen and R. A. W. Haddon, "Earth Models Based on Compressibility Theory," Phys. Earth Planet. Interiors 1, 1-13 (1967).

9. B. Gutenberg and C. F. Richter, "Magnitude and Energy of Earthquakes," Ann. di Geofis. 9, 1-15 (1956).
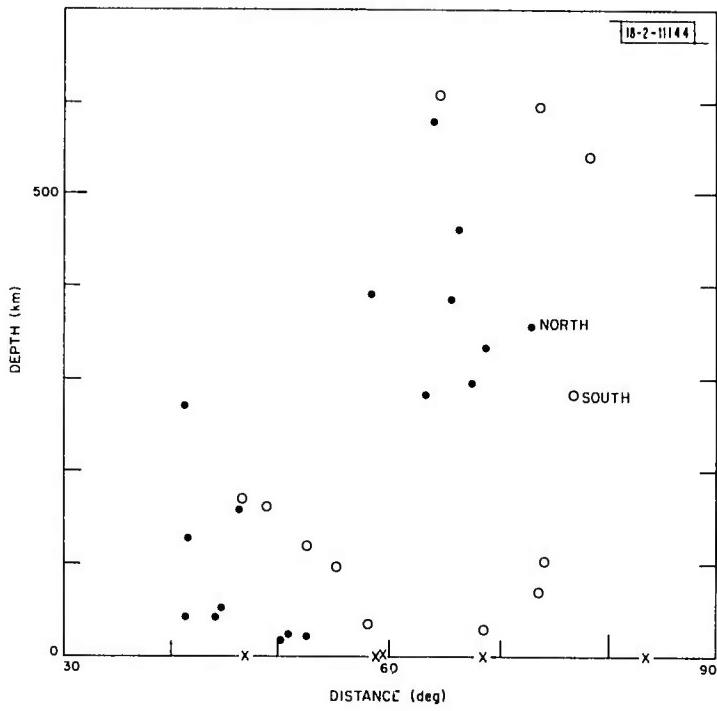
Fig. V-1.   Distribution of data in depth and distance from LASA.   Open circles
are events southeast of LASA; solid circles are events northwest of LASA.
Presumed explosions are denoted by x's and are all northwest to north of LASA.
These symbols are used on all subsequent data figures.
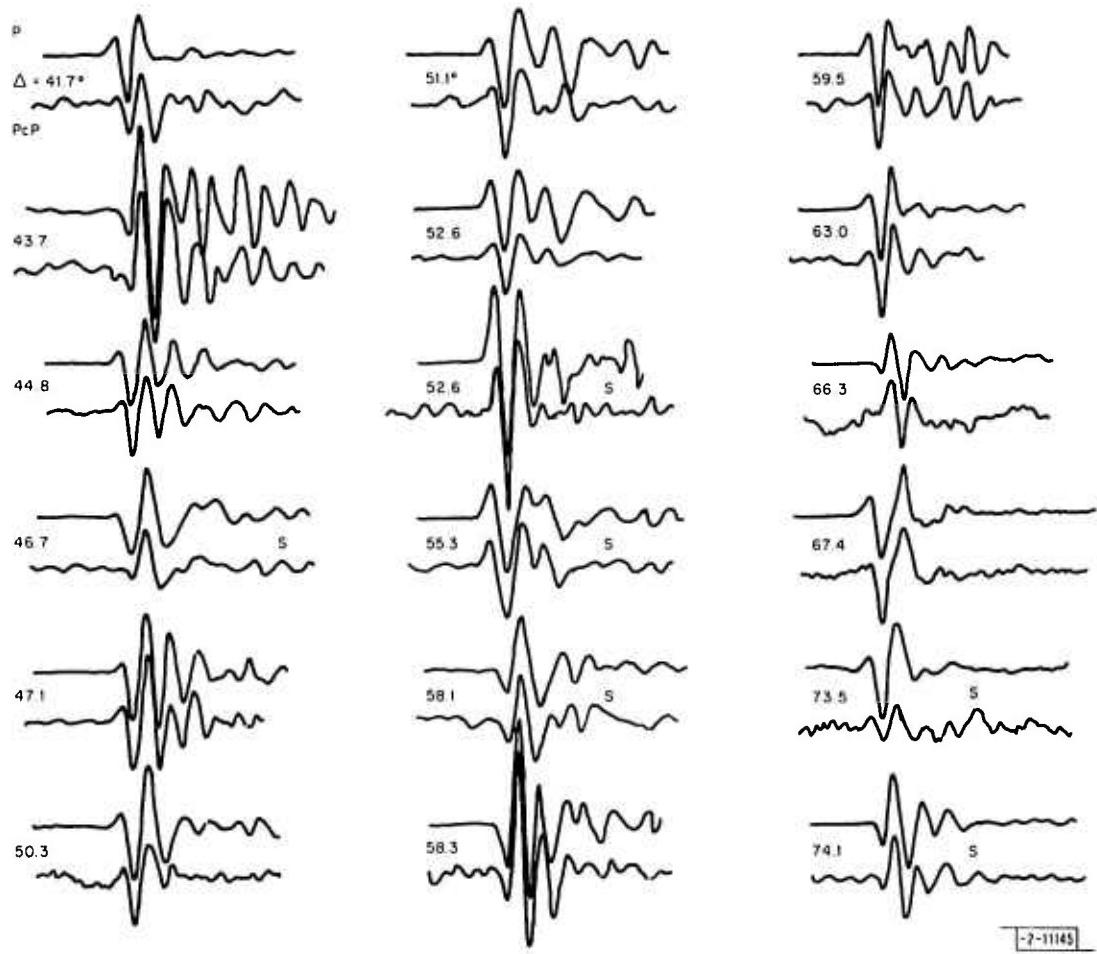
Fig. V-2. P and PcP beams of approximately one-half of data studied. Events marked S are southeast of LASA, all others being northwest of LASA.
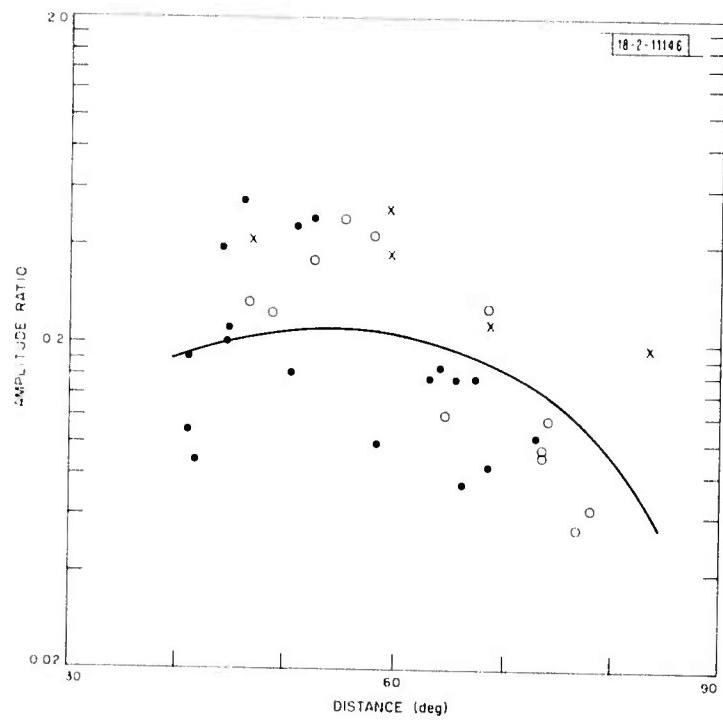
Fig. V-3. PcP/P amplitude ratios as a function of distance from LASA. Amplitudes are n/sec, corrected for instrument response. Curve is theoretical ratio expected for nonattenuative earth model described in text.
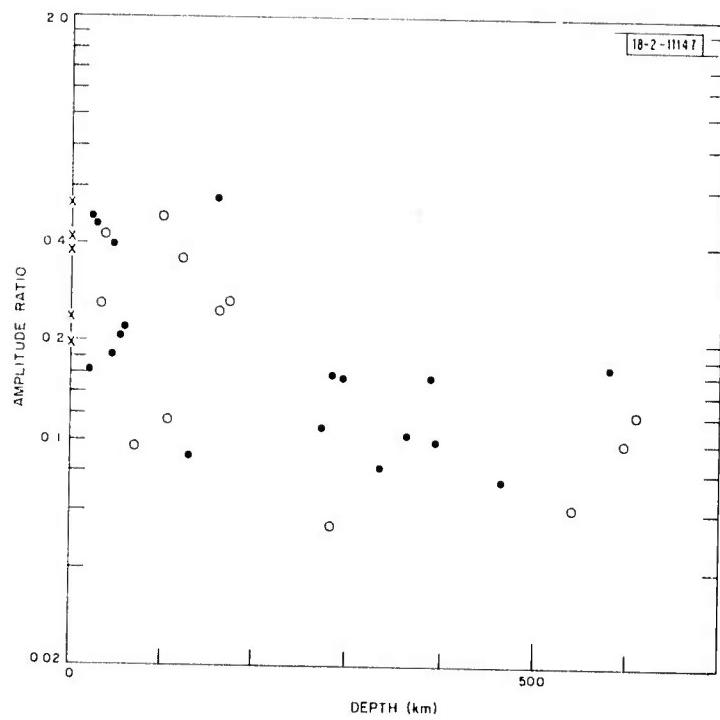
Fig. V-4. PcP/P ratios plotted as a function of depth of focus.
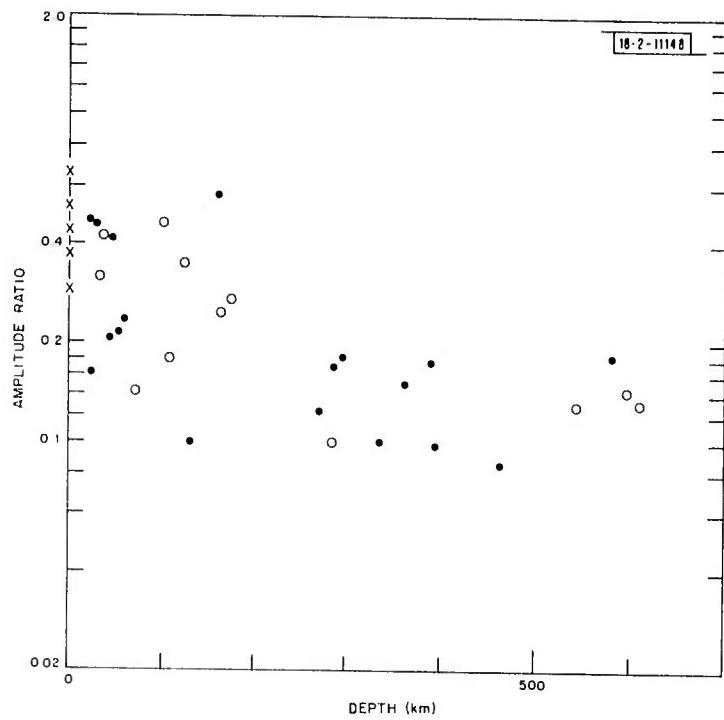
Fig. V-5. PcP/P ratios normalized to $\Delta = 60°$, by removing trend of curve in Fig. V-3.
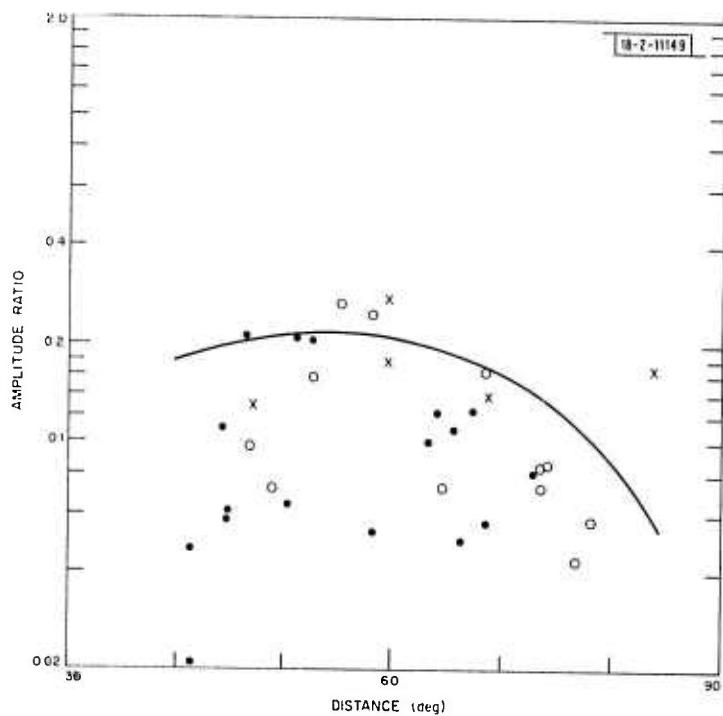
Fig. V-6. PcP/P ratios corrected for differential attenuation of P and PcP using Kanamori's Q model.
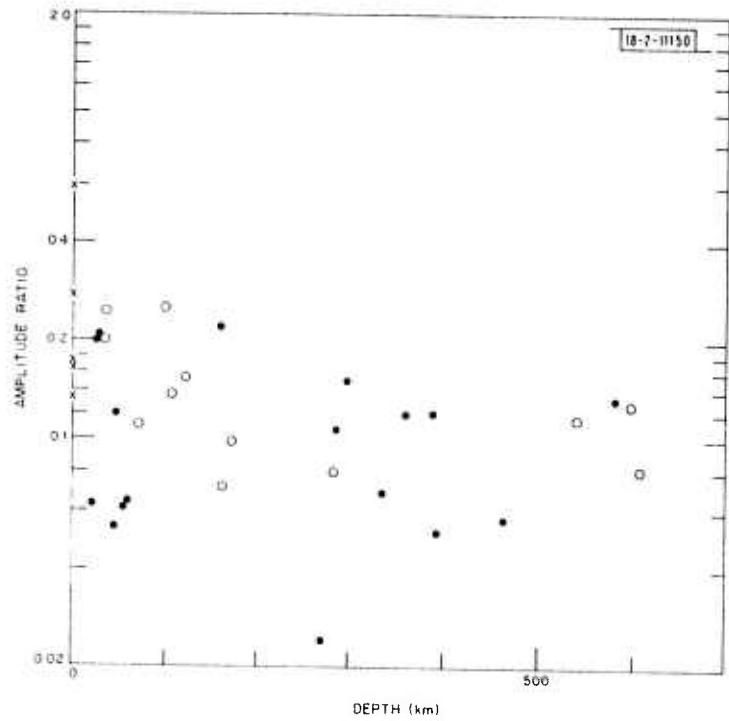
Fig. V-7. PcP/P ratios corrected for Kanamori's Q model and normalized to Δ = 60°.
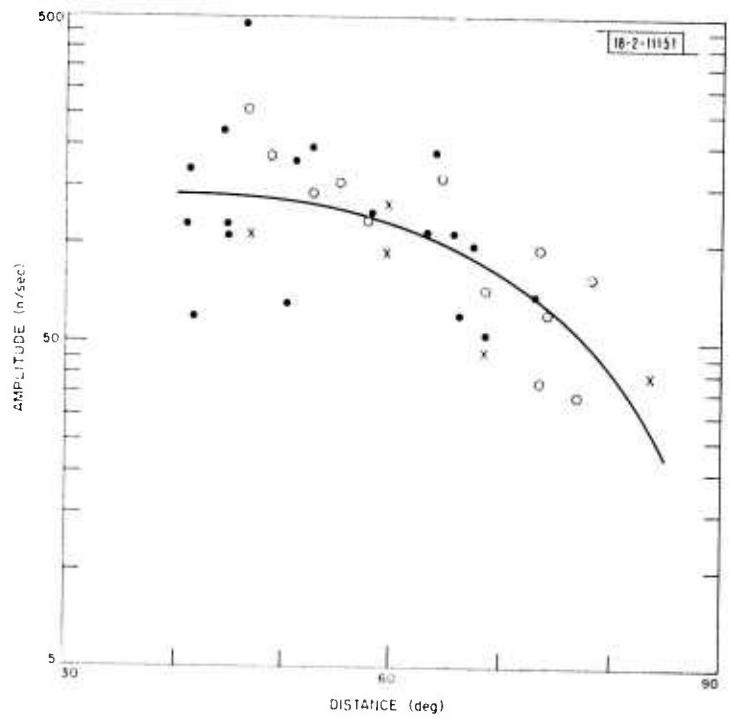

Fig. V-8. PcP amplitudes (n/sec) normalized to LASA m_b = 6.0, as measured on P-waves for each event. Curve is theoretical PcP amplitude assuming un-attenuated earth model.
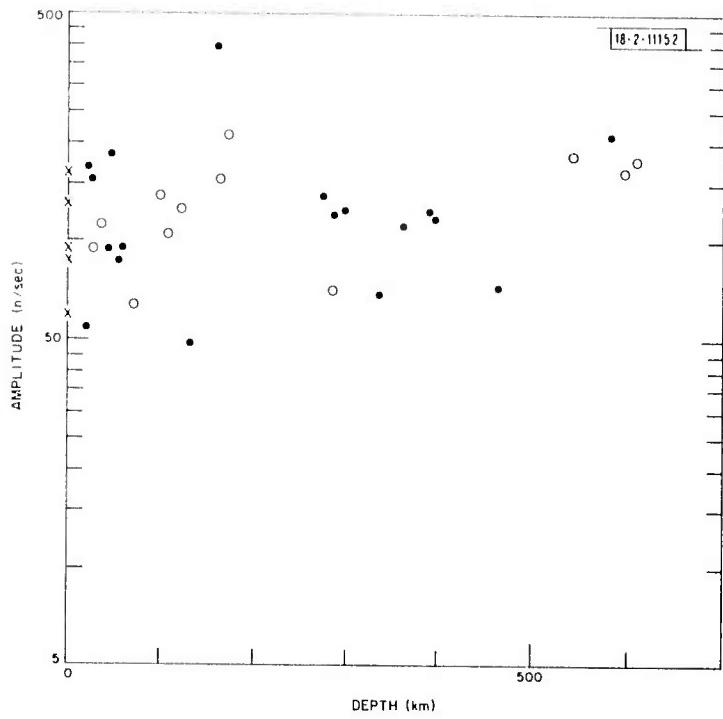
Fig. V-9. PcP amplitudes of Fig. V-8 plotted as a function of depth after removing trend curve.